EUROPEAN ORGANIZATION FOR NUCLEAR RESEARCH

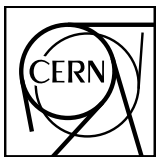

CERN-PH-EP-2012-227
02 August 2012

D_s^+ meson production at central rapidity in proton–proton collisions at $\sqrt{s} = 7$ TeV

The ALICE Collaboration*

Abstract

The p_T-differential inclusive production cross section of the prompt charm-strange meson D_s^+ in the rapidity range $|y| < 0.5$ was measured in proton–proton collisions at $\sqrt{s} = 7$ TeV at the LHC using the ALICE detector. The analysis was performed on a data sample of 2.98×10^8 events collected with a minimum-bias trigger. The corresponding integrated luminosity is $L_{\rm int} = 4.8$ nb^{-1}. Reconstructing the decay $D_s^+ \to \phi\pi^+$, with $\phi \to K^-K^+$, and its charge conjugate, about 480 $D_s^\pm$ mesons were counted, after selection cuts, in the transverse momentum range $2 < p_T < 12$ GeV/c. The results are compared with the prediction of a model based on perturbative QCD. The ratios of the cross sections of four D meson species (namely D^0, D^+, D^{*+} and D_s^+) were determined both as a function of p_T and integrated over p_T after extrapolating to full p_T range, together with the strangeness suppression factor in charm fragmentation. The obtained values are found to be compatible within uncertainties with those measured by other experiments in e^+e^-, ep and pp interactions at various centre-of-mass energies.

*See Appendix A for the list of collaboration members

1 Introduction

The measurement of open charm production in proton–proton (pp) collisions at the Large Hadron Collider (LHC) provides a way to test predictions of quantum chromodynamics (QCD) at the highest available collision energies. Charm and beauty production cross sections can be computed in perturbative QCD (pQCD) using the factorization approach [1, 2]. In this scheme, cross sections are computed as a convolution of three terms: the parton distribution functions of the incoming protons, the partonic hard scattering cross section, and the fragmentation process. The partonic hard scattering cross section is computed through a perturbative calculation [1, 2], while the parton distribution functions and the fragmentation process are parametrized on experimental data. In particular, the fragmentation describes the non-perturbative transition of a charm quark to a hadron. It is modeled by a fragmentation function, which parametrizes the fraction of quark energy transferred to the produced hadron, and by the fragmentation fractions, $f(\mathrm{c} \to \mathrm{D})$, which describe the probability of a charm quark to hadronize into a particular hadron species.

The production of prompt D^0, D^+ and D^{*+} mesons in pp collisions at $\sqrt{s} = 7$ TeV was measured with the ALICE detector at two centre-of-mass energies, namely 7 and 2.76 TeV [3,4]. Here, 'prompt' indicates D mesons produced at the pp interaction point, either directly in the hadronization of the charm quark or in strong decays of excited charm resonances. The contribution from weak decays of beauty mesons, which give rise to feed-down D mesons displaced from the interaction vertex, was subtracted. The measured p_{T}-differential cross sections for prompt D^0, D^+ and D^{*+} are described within uncertainties by theoretical predictions based on pQCD at next-to-leading order (e.g. in the general-mass variable-flavour-number scheme, GM-VFNS [6]) or at fixed order with next-to-leading-log resummation (FONLL [5]). The central value of the GM-VFNS predictions for these three mesons lies systematically above the data. On the other hand, the data tend to be higher than the central value of the FONLL predictions, as it was observed at lower collision energies, namely at the Tevatron [7, 8], where hadronic decays of D mesons were reconstructed, and at RHIC, where measurements of electrons from semileptonic D and B decays were performed [9, 10].

The measurement of the p_{T}-differential prompt D_s^+ meson production is of particular interest due to its strange valence quark content. The D_s^+ production cross section in hadronic collisions was measured at lower energies at the Tevatron collider in the transverse momentum (p_{T}) range $8 < p_{\mathrm{T}} < 12$ GeV/c [7]. Preliminary results for D_s^+ production at the LHC were reported by the LHCb Collaboration for prompt mesons at forward rapidity [11] and by the ATLAS Collaboration at central rapidity [12]. The LHCb Collaboration also measured the asymmetry between prompt D_s^+ and D_s^- production in the rapidity region $2 < y < 4.5$ and for transverse momenta $p_{\mathrm{T}} > 2$ GeV/c, observing a small excess of D_s^- mesons: $A_{\mathrm{P}} = (\sigma(\mathrm{D}_s^+) - \sigma(\mathrm{D}_s^-))/(\sigma(\mathrm{D}_s^+) + \sigma(\mathrm{D}_s^-)) = (-0.33 \pm 0.22 \pm 0.10)\%$ [13]. Such a particle-antiparticle production asymmetry is understood in phenomenological models as due to the effect of the beam remnants on the heavy-quark hadronization, see e.g. [14].

Charm production has been measured in ep interactions at the HERA collider by the ZEUS [15] and H1 [16] Collaborations, as well as in $\mathrm{e}^+\mathrm{e}^-$ annihilations, at the Z^0 resonance, by the ALEPH [17], DELPHI [18] and OPAL [19] Collaborations, and at centre-of-mass energies of about 10 GeV by the CLEO [20] and ARGUS [21] Collaborations.

As far as theoretical models are concerned, a calculation of the D_s^+ production cross section within the FONLL framework is not available, because of the poor knowledge of the parton fragmentation function. The measured data points can be compared with the GM-VFNS prediction that uses meson specific fragmentation functions [22].

From the differential production cross section of prompt D^0, D^+, D^{*+} and D_s^+ mesons, the relative production yields of the D meson species can be studied as a function of transverse momentum. A p_{T} dependence is expected for these ratios, due to differences in the fragmentation function of the charm

quark in the four considered meson species, and because of the different contributions from decays of higher excited states. In this sense, the measurement of the ratios between the D meson species can provide information on the fragmentation functions that can be used in the pQCD models based on the factorization approach. The suppression of strange meson production in the charm fragmentation is quantified by the strangeness suppression factor, γ_s, which is computed from the measured D^0, D^+ and D_s^+ cross sections extrapolated to full p_T range, as defined in Section 6. The values measured at the LHC can be compared with those measured for different energies and different colliding systems [23].

Furthermore, the measurement of D_s^+ in pp collisions provides a reference for the studies of charm production in heavy-ion collisions. According to QCD calculations on the lattice, under the conditions of high energy-density and temperature that are reached in these collisions, the confinement of quarks and gluons into hadrons vanishes and a transition to a Quark-Gluon Plasma (QGP) occurs [24]. Charm hadrons are a powerful tool to study the properties of the QCD medium created in these collisions [25–27]. In particular, the D_s^+ meson is sensitive to strangeness production in heavy-ion collisions. Strange quarks are abundant in the QGP, resulting in an enhanced production of strange particles with respect to pp collisions [28–31]. Hence, at low momentum, the relative yield of D_s^+ mesons with respect to non-strange charm mesons (such as D^0 and D^+) is predicted to be enhanced in nucleus-nucleus collisions [32–34], if the dominant mechanism for D meson formation at low/intermediate momenta is in-medium hadronization of charm quarks via coalescence with strange quarks [35–37].

In this paper, we report on the measurement of D_s^+ production cross section in pp collisions at $\sqrt{s} = 7$ TeV with the ALICE detector at the LHC. D_s^+ mesons were reconstructed through their hadronic decay channel $D_s^+ \to \phi\pi^+$ with a subsequent decay $\phi \to K^-K^+$. The p_T-differential cross section is measured over a range of transverse momentum extending from 2 GeV/c up to 12 GeV/c at central rapidity, $|y| < 0.5$. In Section 2, the detector layout and the data sample are described. This is followed, in Section 3, by the description of the D_s^+ meson reconstruction strategy, the selection cuts, and the raw yield extraction from the invariant mass distributions. The various corrections applied to obtain the production cross sections are illustrated in Section 4. This also includes the estimation of the fraction of promptly produced D_s^+ mesons. The various sources of systematic uncertainties are discussed in detail in Section 5. The results on the p_T-differential cross section compared with pQCD theoretical predictions, the D meson production ratios, and the strangeness suppression factor are presented in Section 6.

2 Detector layout and data collection

The ALICE detector is described in detail in [38]. It is composed of a central barrel, a forward muon spectrometer, and a set of forward detectors for triggering and event characterization. The detectors of the central barrel are located inside a large solenoid magnet that provides a magnetic field B = 0.5 T, parallel to the beam line.

D_s^+ mesons, and their charge conjugates, were reconstructed in the central rapidity region from their decays into three charged hadrons ($K^-K^+\pi^+$), utilizing the tracking, vertexing and particle identification capabilities of the central barrel detectors.

The trajectories of the decay particles were reconstructed from their hits in the Inner Tracking System (ITS) and in the Time Projection Chamber (TPC) detectors in the pseudo-rapidity range $|\eta| < 0.8$. The ITS [39] consists of six cylindrical layers of silicon detectors with radii in the range between 3.9 cm and 43.0 cm. The two innermost layers are equipped with Silicon Pixel Detectors (SPD), Silicon Drift Detectors (SDD) are used in the two intermediate layers, while the two outermost layers are composed of double-sided Silicon Strip Detectors (SSD). The ITS, thanks to the high spatial resolution of the reconstructed hits, the low material budget (on average 7.7% of a radiation length for tracks at $\eta = 0$), and the small distance of the innermost layer from the beam vacuum tube, provides the capability to detect the secondary vertices originating from heavy flavour decays. For this purpose, a key role is

played by the two layers of SPD detectors, which are located at radial positions of 3.9 and 7.6 cm from the beam line and cover the pseudo-rapidity ranges $|\eta| < 2.0$ and $|\eta| < 1.4$, respectively. The TPC [40] provides track reconstruction with up to 159 space points per track in a cylindrical active volume of about 90 m^3. The active volume has an inner radius of about 85 cm, an outer radius of about 250 cm, and an overall length along the beam direction of 500 cm.

Particle identification (PID) is provided by the measurement of the specific ionization energy loss, dE/dx, in the TPC and of the flight time in the time-of-flight (TOF) detector. The dE/dx samples measured by the TPC are reduced, by means of a truncated mean, to a Gaussian distribution with a resolution of $\sigma_{dE/dx}/(dE/dx) \approx 5.5\%$ [40]. The TOF detector is positioned at 370–399 cm from the beam axis and covers the full azimuth for the pseudo-rapidity range $|\eta| < 0.9$. The particle identification is based on the difference between the measured time-of-flight and its expected value, computed for each mass hypothesis from the track momentum and length. The overall resolution on this difference is about 160 ps and it includes the detector intrinsic resolution, the contribution from the electronics and the calibration, the uncertainty on the start time of the event (i.e. the time of the collision), and the tracking and momentum resolution. The start time of the event is defined as the weighted average between the one estimated using the particle arrival times at the TOF [41] and the one measured by the T0 detector. The T0 detector is composed of two arrays of Cherenkov counters located on either side of the interaction point at $+350$ cm and -70 cm from the nominal vertex position along the beam-line. In this analysis, the time-of-flight measurement provides kaon/pion separation up to a momentum of about 1.5 GeV/c.

The data sample used for the analysis consists of 298 million minimum-bias (MB) pp collisions at $\sqrt{s} = 7$ TeV, corresponding to an integrated luminosity $L_{\rm int} = 4.8$ nb^{-1}, collected during the 2010 LHC run period. The minimum-bias trigger was based on the information of the SPD and the VZERO detectors. The VZERO detector is composed of two arrays of scintillator tiles with full azimuthal coverage in the pseudo-rapidity regions $2.8 < \eta < 5.1$ and $-3.7 < \eta < -1.7$. Minimum-bias collisions were triggered by requiring at least one hit in either of the VZERO counters or in the SPD ($|\eta| < 2$), in coincidence with the arrival of proton bunches from both directions. This trigger was estimated to be sensitive to about 87% of the pp inelastic cross section [42, 43]. It was verified by means of Monte Carlo simulations based on the PYTHIA 6.4.21 event generator [44] (with Perugia-0 tune [45]) that the minimum-bias trigger is 100% efficient for events containing D mesons with $p_{\rm T} > 1$ GeV/c and $|y| < 0.5$ [3]. Events were further selected offline to remove the contamination from beam-induced background using the timing information from the VZERO and the correlation between the number of hits and track segments (tracklets) in the SPD detector.

During the pp run, the luminosity in the ALICE experiment was limited to 0.6–1.2×10^{29} $cm^{-2}s^{-1}$ by displacing the beams in the transverse plane by 3.8 times the r.m.s. of their transverse profile, thus keeping the probability of collision pile-up below 4% per triggered event. The luminous region, measured from the distribution of the reconstructed interaction vertices, had an r.m.s. width of about 4–6 cm along the beam direction and 35–50 μm in the transverse plane (the quoted ranges originate from the variations of the beam conditions during the data taking). Only events with a vertex found within ± 10 cm from the centre of the detector along the beam line were used for the analysis. This requirement selects a region where the vertex reconstruction efficiency is independent of its position along the beam line and it provides almost uniform acceptance for particles within the pseudo-rapidity range $|\eta| < 0.8$ for all events in the analyzed sample. Pile-up events were identified by the presence of more than one interaction vertex reconstructed by matching hits in the two SPD layers (tracklets). An event was rejected from the analyzed data sample if a second interaction vertex was found, it had at least 3 associated tracklets, and it was separated from the first one by more than 8 mm. The remaining undetected pile-up is negligible for the analysis described in this paper.

3 D_s^+ meson reconstruction and selection

D_s^+ mesons and their antiparticles were reconstructed in the decay chain $D_s^+ \to \phi\pi^+$ (and its charge conjugate) followed by $\phi \to K^-K^+$. The branching ratio (BR) of the chain $D_s^+ \to \phi\pi^+ \to K^-K^+\pi^+$ is $2.28 \pm 0.12\%$ [46]. It should be noted that other D_s^+ meson decay channels can give rise to the same $K^-K^+\pi^+$ final state. Among them, those with larger BR are $D_s^+ \to \overline{K}^{*0}K^+$ and $D_s^+ \to f_0(980)\pi^+$, with BR into the $K^-K^+\pi^+$ final state of $2.63 \pm 0.13\%$ and $1.16 \pm 0.32\%$, respectively. However, as it will be discussed in the following, the selection efficiency for these decay modes is strongly suppressed by the cuts applied to select the signal candidates, and therefore the measured yield is dominated by the $D_s^+ \to \phi\pi^+ \to K^-K^+\pi^+$ decays.

D_s^+ mesons have a mean proper decay length $c\tau = 150 \pm 2$ μm [46], which makes it possible to resolve their decay vertex from the interaction (primary) vertex. The analysis strategy for the extraction of the signal from the large combinatorial background can therefore be based on the reconstruction and selection of secondary vertex topologies with significant separation from the primary vertex.

D_s^+ meson candidates were defined from triplets of tracks with proper charge sign combination. Tracks were selected requiring $|\eta| < 0.8$, $p_T > 0.4$ GeV/c, a minimum of 70 associated space points in the TPC, $\chi^2/\mathrm{ndf} < 2$ for the track momentum fit in the TPC, and at least 2 associated hits in the ITS, out of which at least one has to be in either of the two SPD layers. For tracks that satisfy these TPC and ITS selection criteria, the transverse momentum resolution is better than 1% at $p_T = 1$ GeV/c and about 2% at $p_T = 10$ GeV/c. The resolution on the track impact parameter (i.e. the distance of closest approach of the track to the primary interaction vertex) in the bending plane ($r\phi$) is better than 75 μm for $p_T > 1$ GeV/c, well reproduced in Monte Carlo simulations [3].

For each D_s^+ candidate, in order to have an unbiased estimate of the interaction vertex, the event primary vertex was recalculated from the reconstructed tracks after excluding the candidate decay tracks. The secondary vertex was reconstructed from the decay tracks with the same algorithm used to compute the primary vertex [3]. The position resolution on the D_s^+ decay vertices was estimated via Monte Carlo simulations to be of the order of 100 μm for each of the three coordinates with little dependence on p_T. The resolution on the position of the primary vertex depends on the event multiplicity: for the transverse coordinates, where the information on the position and spread of the luminous region is used to constrain the vertex fit, it ranges from 40 μm in low-multiplicity events to about 10 μm in events with 40 charged particles per unit of rapidity.

Candidates were then filtered by applying kinematical and topological cuts together with particle identification criteria. With the track selection described above, the acceptance in rapidity for D mesons drops steeply to zero for $|y| \gtrsim 0.5$ at low p_T and $|y| \gtrsim 0.8$ at $p_T \gtrsim 5$ GeV/c. A p_T-dependent fiducial acceptance cut was therefore applied on the D meson rapidity, $|y| < y_{\mathrm{fid}}(p_T)$, where p_T is the D_s^+ transverse momentum. The cut value, $y_{\mathrm{fid}}(p_T)$, increases from 0.5 to 0.8 in the transverse momentum range $0 < p_T < 5$ GeV/c according to a second-order polynomial function and it takes a constant value of 0.8 for $p_T > 5$ GeV/c.

The topological selections were tuned to have a large statistical significance of the signal, while keeping the selection efficiency as high as possible. It was also checked that background fluctuations were not causing a distortion in the signal line shape by verifying that the D_s^+ meson mass and its resolution were in agreement with the Particle Data Group (PDG) value (1.969 GeV/c^2 [46]) and the simulation results, respectively. The resulting cut values depend on the transverse momentum of the candidate.

The candidates were selected according to the decay length and the cosine of the pointing angle, which is the angle between the reconstructed D meson momentum and the line connecting the primary and secondary vertex. The three tracks composing the candidate triplet were required to have small distance to the reconstructed decay vertex. In addition, D_s^+ candidates were selected by requiring that one of the

Table 1: Measured raw yields, signal (S) over background (B) and statistical significance ($S/\sqrt{S+B}$) for D_s^+ and their antiparticles in the four considered p_T intervals. The estimation of the systematic uncertainty on the raw yield is described in Section 5.

p_T interval (GeV/c)	$N^{D_s^\pm \text{ raw}} \pm \text{stat.} \pm \text{syst.}$	S/B (3σ)	Significance (3σ)
2–4	125±36±25	0.12	3.6
4–6	189±35±28	0.26	6.3
6–8	79±19±12	0.40	4.8
8–12	85±16±17	0.58	5.6

two pairs of opposite-charged tracks has an invariant mass compatible with the PDG world average for the ϕ mass (1.019 GeV/c^2 [46]). To further suppress the combinatorial background, the angles $\theta^*(\pi)$ and $\theta'(\mathrm{K})$ were exploited. $\theta^*(\pi)$ is the angle between the pion in the KKπ rest frame and the KKπ flight line, which is defined by the positions of the primary and secondary vertices in the laboratory frame. $\theta'(\mathrm{K})$ is the angle between one of the kaons and the pion in the KK rest frame. The cut values used for the D_s^+ mesons with $2 < p_T < 4$ GeV/c were: decay length larger than 350 μm, $\cos\theta_{\text{pointing}} > 0.94$, $|M^{\text{inv}}_{K^+K^-} - M^{\text{PDG}}_{\phi}| < 8$ MeV/c^2, $\cos\theta^*(\pi) < 0.95$, and $|\cos^3\theta'(\mathrm{K})| > 0.1$. A looser selection was applied at higher p_T due to the lower combinatorial background, resulting in a selection efficiency that increases with increasing p_T.

Particle identification selections, based on the specific energy loss, dE/dx, from the TPC and the time-of-flight from the TOF detector, were used to obtain further reduction of the background. Compatibility cuts were applied to the difference between the measured signals and those expected for a pion or a kaon. A track was considered compatible with the kaon or pion hypothesis if both its dE/dx and time-of-flight were within 3σ from the expected values, with at least one of them within 2σ. Tracks without a TOF signal were identified using only the TPC information and requiring a 2σ compatibility with the expected dE/dx. Candidate triplets were required to have two tracks compatible with the kaon hypothesis and one with the pion hypothesis. In addition, since the decay particle with opposite charge sign has to be a kaon, a triplet was rejected if the opposite-sign track was not compatible with the kaon hypothesis. This particle identification strategy preserves more than 90% of the D_s^+ signal and provides a reduction of the combinatorial background under the D_s^+ peak by a factor of 10 in the lowest p_T interval ($2 < p_T < 4$ GeV/c), a factor of 5 in $4 < p_T < 6$ GeV/c and a factor of 2 at higher transverse momenta.

For each candidate, two values of invariant mass can be computed, corresponding to the two possible assignments of the kaon and pion mass to the two same-sign tracks. Signal candidates with wrong mass assignment to the same-sign tracks would give rise to a contribution to the invariant mass distributions that could potentially introduce a bias in the measured raw yield of D_s^+ mesons. It was verified, both in data and in simulations, that this contribution is reduced to a negligible level by the particle identification selection and by the requirement that the invariant mass of the two tracks identified as kaons is compatible with the ϕ PDG mass.

The raw signal yields were extracted by fitting the invariant mass distributions in each p_T interval as shown in Fig. 1. The fitting function consists of a sum of a Gaussian and an exponential function to describe the signal and the background, respectively. For all p_T intervals, the invariant mass range used for the fit was $1.88 < M^{\text{inv}}_{KK\pi} < 2.16$ GeV/c^2, chosen in order to exclude the region where the background shape is affected by $D^+ \to K^-K^+\pi^+$ decays (BR=0.265% [46]) that give rise to a bump at the D^+ invariant mass (1.870 GeV/c^2 [46]). The mean values of the Gaussian functions in all transverse momentum intervals were found to be compatible within the uncertainties with the PDG world average for the D_s^+ mass. The Gaussian widths are well reproduced in Monte Carlo simulations. In Table 1 the extracted raw yields of D_s^+ meson (sum of particle and antiparticle) are reported for the different p_T intervals, together with the signal-over-background (S/B) ratios and the statistical

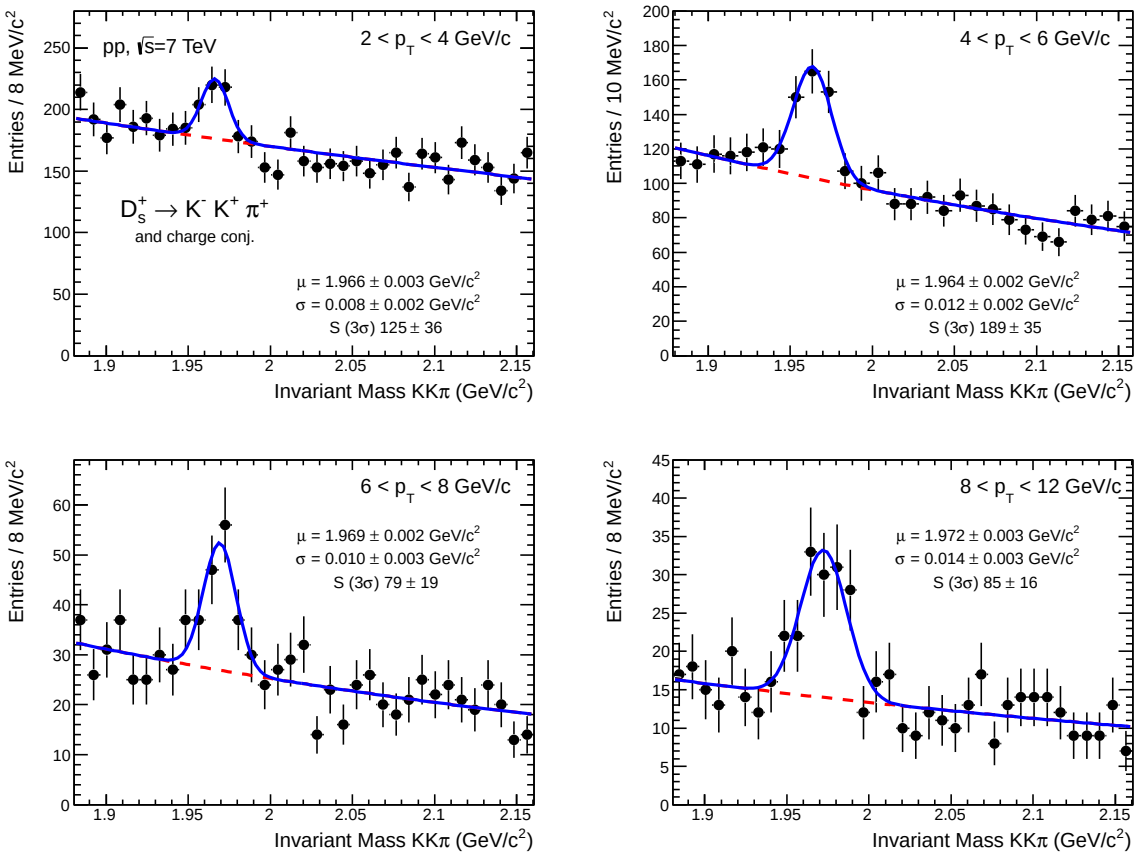

Figure 1: Invariant mass distributions for D_s^+ candidates and charge conjugates in the four considered p_T intervals. The fit functions described in the text are also shown. The values of mean (μ) and width (σ) of the signal peak are reported together with the signal counts (S).

significance, $S/\sqrt{S+B}$, with signal and background evaluated by integrating the fit functions in $\pm 3\sigma$ around the centroid of the Gaussian.

4 Corrections

In order to obtain the p_T-differential cross section for prompt (i.e. not coming from weak decays of beauty mesons) $D_s^\pm$ mesons, the raw yields obtained from the invariant mass analysis ($N^{D_s^\pm\ \mathrm{raw}}$) were corrected for the experimental acceptance, the reconstruction and selection efficiency, and for the contribution to the D_s^+ measured yield from B meson decay feed-down. The production cross section of prompt D_s^+ mesons was computed as:

$$\left.\frac{\mathrm{d}\sigma^{D_s^+}}{\mathrm{d}p_T}\right|_{|y|<0.5} = \frac{1}{2}\frac{1}{\Delta y \Delta p_T}\frac{f_{\mathrm{prompt}} \cdot N^{D_s^\pm\ \mathrm{raw}}\Big|_{|y|<y_{\mathrm{fid}}}}{(\mathrm{Acc}\times\varepsilon)_{\mathrm{prompt}} \cdot \mathrm{BR} \cdot L_{\mathrm{int}}}. \quad (1)$$

where Δp_T is the width of the p_T interval, Δy ($= 2y_{\mathrm{fid}}(p_T)$) is the width of the fiducial rapidity coverage (see Section 3) and BR is the decay branching ratio (2.28% [46]). The factor f_{prompt} is the prompt fraction of the raw yield; $(\mathrm{Acc}\times\varepsilon)_{\mathrm{prompt}}$ is the acceptance times efficiency of promptly produced D_s^+ mesons. The efficiency ε accounts for vertex reconstruction, track reconstruction and selection, and for D_s^+ candidate selection with the topological and particle identification criteria described in Section 3.

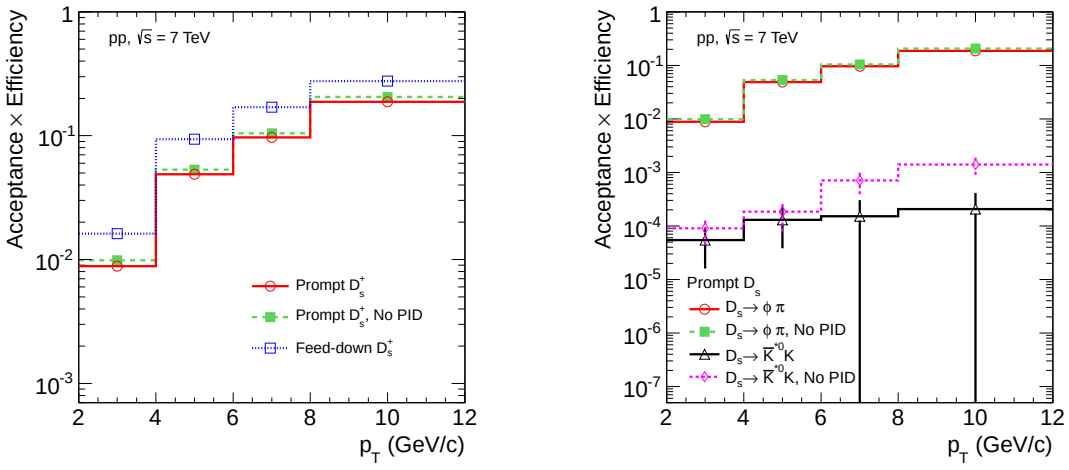

Figure 2: Acceptance × efficiency for D_s^+ mesons as a function of p_T, for prompt and feed-down D_s^+ mesons (left panel) and decays through ϕ and $\overline{K}^{*0}$ intermediate resonant state (right panel).

The factor $1/2$ accounts for the fact that the measured raw yields are the sum of D_s^+ and D_s^-, while the cross section is given for particles only, neglecting the small particle-antiparticle production asymmetry observed by LHCb [13]. The integrated luminosity, $L_{\rm int} = 4.8$ nb^{-1}, was computed from the number of analyzed events and the cross section of pp collisions passing the minimum-bias trigger condition defined in Section 2, $\sigma_{\rm pp,MB} = 62.2$ mb [43, 47]. The value of $\sigma_{\rm pp,MB}$ was derived from a van der Meer scan [48] measurement, which has an uncertainty of 3.5%, mainly due to the uncertainties on the beam intensities.

The acceptance and efficiency correction factors were determined using pp collisions simulated with the PYTHIA 6.4.21 event generator [44] with the Perugia-0 tune [45]. Only events containing D mesons were transported through the apparatus (using the GEANT3 transport code [49]) and reconstructed. The luminous region distribution and the conditions (active channels, gain, noise level, and alignment) of all the ALICE detectors were included in the simulations, considering also their evolution with time during the 2010 LHC run.

The acceptance-times-efficiency for $D_s^+ \to \phi\pi^+ \to K^-K^+\pi^+$ decays in the fiducial rapidity range described in Section 3 are shown in the left panel Fig. 2 for prompt and feed-down D_s^+ mesons. The acceptance-times-efficiency for the prompt mesons increases from about 1% in the lowest considered p_T interval up to 10–15% at high p_T. For D_s^+ mesons from B decays, the efficiency is larger by a factor 1.5–2 (depending on p_T) because the decay vertices of the feed-down D mesons are more displaced from the primary vertex and, therefore, they are more efficiently selected by the topological cuts. The difference between the prompt and feed-down efficiencies decreases with increasing p_T, because the applied selections are looser in the higher transverse momentum intervals. The acceptance-times-efficiency for prompt D_s^+ mesons obtained without applying the particle identification selection is also shown to single out the PID contribution to the overall efficiency. The used particle identification strategy preserves more than 90% of the signal and does not show any significant dependence on D_s^+ meson p_T in the range considered in this analysis.

As discussed in Section 3, the decay of the D_s^+ meson into the $K^-K^+\pi^+$ final state occurs via different intermediate resonant states. The selection strategy used in this analysis requires that one of the opposite-sign pairs of tracks composing the candidate triplet has an invariant mass compatible with the ϕ meson. The decays $D_s^+ \to \phi\pi^+ \to K^-K^+\pi^+$ are therefore preferentially selected by the applied cuts. Nevertheless, a fraction of the D_s^+ decaying via another resonant state can pass the selection cuts. In the

right panel of Fig. 2, the acceptance-times-efficiencies for prompt D_s^+ decaying to $K^-K^+\pi^+$ final state via a ϕ and a $\overline{K}^{*0}$ in the intermediate state are compared. The acceptance-times-efficiency for the decay chain $D_s^+ \to \overline{K}^{*0}K^+ \to K^-K^+\pi^+$ is smaller by a factor $\approx$ 100 with respect to the decay through ϕ, and it is further reduced when applying the PID selection. Indeed, the PID allows the rejection of D_s^+ decaying via a $\overline{K}^{*0}$ that would pass the selection on the invariant mass of the ϕ in case of wrong assignment of the mass (kaon/pion) to the two same-sign tracks.

The contribution to the inclusive raw yields due to D_s^+ from B feed-down was subtracted using the beauty production cross section from the FONLL calculation [1, 5], the B$\to D_s^+$ decay kinematics from the EvtGen package [50], and the Monte Carlo efficiencies for feed-down D_s^+ mesons. Before running the EvtGen decayer, the B admixture cross section predicted by FONLL was split into that of B^0, B^+, B_s^0 and Λ_b by assuming the same p_T shape for all hadrons and the production fractions from [46], namely 40.1% of B^0, 40.1% of B^+, 10.5% of B_s^0 and 9.3% of beauty baryons. The resulting fraction of prompt D_s^+ mesons, $f_{\rm prompt}$, depends on the p_T interval, on the applied selection cuts, and on the parameters used in the FONLL calculation for the B meson cross section. It ranges from 0.93 in the lowest transverse momentum interval ($2 < p_T < 4$ GeV/c) to ≈ 0.87 at high p_T (> 6 GeV/c).

5 Systematic uncertainties

The systematic uncertainties on the D_s^+ cross section are summarized in Table 2 for the considered p_T intervals.

The systematic uncertainty on the yield extraction was defined as the full spread of the D_s^+ yield values obtained with different techniques to analyze the invariant mass distributions in each p_T interval. The fit was repeated in different mass ranges and by varying the function used to describe the background. In particular, first and second order polynomials were used instead of an exponential for the background. In case of fitting in an extended mass range, a second Gaussian signal was included in the fit function to account for the $D^+ \to K^-K^+\pi^+$ decays. Furthermore, the yield extraction was repeated using a method based on bin counting after subtraction of the background estimated from a fit in the mass side bands. The resulting uncertainty amounts to 15–20% depending on the p_T interval, as detailed in Table 2.

The systematic uncertainty on the tracking efficiency (including the effect of the track selection) was evaluated by comparing the probability of track finding in the TPC and track prolongation from the TPC to the ITS in the data with those in the simulation, and by varying the track quality selections. The estimated uncertainty is 4% per track, which results in 12% for the three-body decay of D_s^+ mesons.

Another source of systematic uncertainty originates from the residual discrepancies between data and simulation for the variables used to select the D_s^+ candidates. The distributions of these variables were compared for candidates passing loose topological cuts, i.e. essentially background candidates, and found to be well described in the simulation. The effect of the imperfect implementation of the detector description in the Monte Carlo simulations was estimated by repeating the analysis with different sets of cuts. The cut values were changed in order to vary the efficiency of signal selection by at least 20% in all p_T intervals. A systematic uncertainty of 15% was estimated from the spread of the resulting corrected yields. Part of this uncertainty is due to residual detector misalignment effects not fully described in the simulation. To estimate this contribution, the secondary vertices in the simulation were reconstructed also after a track-by-track scaling of the impact parameter residuals with respect to their true value. In particular, a scaling factor of 1.08, tuned to reproduce the impact parameter resolution observed in the data (see [3]), was used. The resulting variation of the efficiency was found to be 4% in the lowest p_T interval used in this analysis and less than 1% for $p_T > 6$ GeV/c. This contribution was not included explicitly in the systematic uncertainty, because it is already accounted for in the cut variation study.

Due to the limited statistics, it was not possible to analyze separately D_s^+ and D_s^- candidates to verify the

absence of biases coming from a different reconstruction efficiency for tracks with positive and negative charge sign not properly described in the simulation [1]. This check was carried out for other D meson species [3] without observing any significant difference between particle and antiparticle.

The systematic uncertainty induced by a different efficiency for particle identification in data and simulation was evaluated by comparing the resulting p_{T}-differential cross section with that obtained using a different PID approach based on 3σ (instead of 2σ) cuts on TPC $\mathrm{d}E/\mathrm{d}x$ and time-of-flight signals, which preserves almost 100% of the signal. In addition, the PID efficiency, was estimated by comparing the reduction of signal yield due to the PID selection in data and in simulation, when the same topological cuts are applied. Due to the limited statistical significance, this check could be performed in data only for $\mathrm{D_s^+}$ candidates integrated over the transverse momentum range $4 < p_{\mathrm{T}} < 12$ GeV/c. From these studies, a systematic uncertainty of 7%, independent of p_{T}, was assigned to the PID selection.

The contribution to the measured yield from $\mathrm{D_s^+}$ decaying into the $\mathrm{K^-K^+\pi^+}$ final state via other resonant channels (i.e. not via a ϕ meson) was found to be less than 1% due to the much lower selection efficiency, as shown in the right panel of Fig. 2 for the case of the decay through a $\overline{\mathrm{K}}^{*0}$. The contamination from other decay chains (all having smaller branching ratio than the two reported in Fig. 2) was also found to be negligible.

The effect on the selection efficiency due to the shape of the $\mathrm{D_s^+}$ p_{T} spectrum used in the simulation was estimated from the relative difference between the Monte Carlo efficiencies obtained using two different p_{T} shapes, namely those from PYTHIA [44] with Perugia-0 tune [45] and from the FONLL pQCD calculation [1, 5]. The resulting contribution to the systematic uncertainty was found to be 3% in the two lowest p_{T} intervals, where the selection efficiency is strongly p_{T} dependent, and 2% at higher p_{T}.

The systematic uncertainty from the subtraction of feed-down D mesons was estimated following the same approach as used for $\mathrm{D^0}$, $\mathrm{D^+}$ and $\mathrm{D^{*+}}$ mesons [3]. The contribution of the FONLL perturbative uncertainties was included by varying the heavy-quark masses and the factorization and renormalization scales, μ_{F} and μ_{R}, independently in the ranges $0.5 < \mu_{\mathrm{F}}/m_{\mathrm{T}} < 2$, $0.5 < \mu_{\mathrm{R}}/m_{\mathrm{T}} < 2$, with the constraint $0.5 < \mu_{\mathrm{F}}/\mu_{\mathrm{R}} < 2$, where $m_{\mathrm{T}} = \sqrt{p_{\mathrm{T}}^2 + m_{\mathrm{c}}^2}$. The mass of the b quark was varied within $4.5 < m_{\mathrm{b}} < 5$ GeV/c^2. The uncertainty related to the B decay kinematics was estimated from the difference between the results obtained using PYTHIA [44] instead of EvtGen [50] for the particle decays and was found to be negligible with respect to the uncertainty on the B meson cross section in FONLL. Furthermore, the prompt fraction obtained in each p_{T} interval was compared with the results of a different procedure in which the FONLL cross sections for prompt and feed-down D mesons and their respective Monte Carlo efficiencies are the input for evaluating the correction factor. Since FONLL does not have a specific prediction for $\mathrm{D_s^+}$ mesons, four different approaches were used to compute the p_{T}-differential cross section of promptly produced $\mathrm{D_s^+}$. The first two approaches used the FONLL prediction for the generic admixture of charm hadrons and that for $\mathrm{D^{*+}}$ mesons (the $\mathrm{D^{*+}}$ mass being close to that of the $\mathrm{D_s^+}$) scaled with the fragmentation fractions of charm quarks in the different hadronic species, $f(\mathrm{c} \to \mathrm{D})$, measured by ALEPH [17]. The other two predictions for prompt $\mathrm{D_s^+}$ were computed using the p_{T}-differential cross section of c quarks from FONLL, the fractions $f(\mathrm{c} \to \mathrm{D})$ from ALEPH [17], and the fragmentation functions from [51], which have one parameter, r. Two definitions were considered for the r parameter: i) $r = (m_{\mathrm{D}} - m_{\mathrm{c}})/m_{\mathrm{D}}$ (m_{D} and m_{c} being the masses of the considered D meson species and of the c quark, respectively) as proposed in [51]; ii) $r = 0.1$ for all mesons, as done in FONLL after fitting the analytical forms of [51] to the $\mathrm{D^{*+}}$ fragmentation function measured by ALEPH [52]. The $\mathrm{D_s^{*+}}$ mesons produced in the c quark fragmentation were made to decay with PYTHIA and the resulting $\mathrm{D_s^+}$ were summed to the primary ones to obtain the prompt yield. For all the four predictions used for prompt $\mathrm{D_s^+}$ cross section, the evaluation of f_{prompt} included the FONLL perturbative uncertainties from the variation of the factorization and renormalization scales in the range quoted above and of the c quark

[1] The small particle-antiparticle asymmetry reported by the LHCb Collaboration [13] is negligible in this context.

mass within $1.3 < m_c < 1.7$ GeV$/c^2$. The systematic uncertainty on the B feed-down was defined from the envelope of the resulting values of $f_{\rm prompt}$. The resulting uncertainties in the transverse momentum intervals used in this analysis are about $^{+\,5}_{-17}$% , as it can be seen in Table 2.

Finally, the results have global systematic uncertainties due to the $D_s^+ \to \phi\pi^+ \to K^-K^+\pi^+$ branching ratio (5.3% [46]) and to the determination of the cross section of pp collisions passing the minimum-bias trigger condition (3.5%).

Table 2: Relative systematic uncertainties for the four considered p_T intervals.

	p_T interval (GeV$/c$)			
	2–4	4–6	6–8	8–12
Raw yield extraction	20%	15%	15%	20%
Tracking efficiency	12%	12%	12%	12%
Topological selection efficiency	15%	15%	15%	15%
PID efficiency	7%	7%	7%	7%
MC p_T shape	3%	3%	2%	2%
Other resonant channels	<1%	<1%	<1%	<1%
Feed-down from B	$^{+\,4}_{-18}$%	$^{+\,4}_{-17}$%	$^{+\,6}_{-15}$%	$^{+\,5}_{-17}$%
Branching ratio	5.3%			
Normalization	3.5%			

6 Results

6.1 p_T-differential D_s^+ cross section and D meson ratios

The inclusive production cross section for prompt D_s^+ mesons in four transverse momentum intervals in the range $2 < p_T < 12$ GeV$/c$ is shown in Fig. 3. As discussed in section 4, the cross section reported in Fig. 3 refers to particles only, being computed as the average of particles and antiparticles under the assumption that the production cross section is the same for D_s^+ and D_s^-. The vertical error bars represent the statistical uncertainties, while the systematic uncertainties are shown as boxes around the data points. The symbols are positioned horizontally at the centre of each p_T interval, with the horizontal bars representing the width of the p_T interval. In Table 3, the numerical values of the prompt D_s^+ production cross section are reported together with the average p_T of D_s^+ mesons in each transverse momentum interval. The $\langle p_T \rangle$ values were obtained from the p_T distribution of the candidates in the D_s^+ peak region, after subtracting the background contribution estimated from the side bands of the invariant mass distribution. The measured differential production cross section is compared to the theoretical prediction from the GM-VFNS model [6, 53], which is found to be compatible with the measurements, within the uncertainties. The central value of the GM-VFNS prediction corresponds to the default values of the renormalization (μ_R) and factorization (μ_I and μ_F for initial- and final-state singularities, respectively) scales, i.e. $\mu_R = \mu_I = \mu_F = m_T$, where $m_T = \sqrt{p_T^2 + m_c^2}$, with $m_c = 1.5$ GeV$/c^2$. The theoretical uncertainties are determined by varying the values of the renormalization and factorization scales by a factor of two up and down with the constraint that any ratio of the scale parameters should be smaller than or equal to two [6]. The central value of the GM-VFNS prediction is higher than the measured point by ≈ 50% in the first p_T interval, while in the other intervals it agrees with the data within ≈ 15%. For D^0, D^+ and D^{*+} mesons measured by ALICE at the same pp collision energy [3], the central value of the GM-VFNS predictions was found to lie systematically above the data. As mentioned in Section 1, predictions for the D_s^+ production cross section within the FONLL framework are not available, due to the poor knowledge of the fragmentation function for charm-strange mesons.

The ratios of the p_T-differential cross sections of D^+ and D^{*+} to that of D^0, taken from [3], are shown in

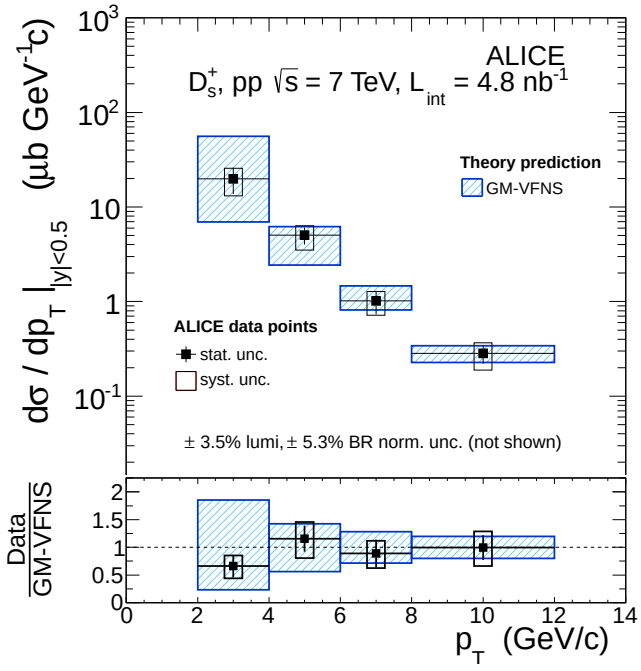

Figure 3: (colour online) $p_{\rm T}$-differential inclusive cross section for prompt D_s^+ meson production in pp collisions at $\sqrt{s} = 7$ TeV. The symbols are positioned horizontally at the centre of each $p_{\rm T}$ interval. The horizontal error bars represent the $p_{\rm T}$ interval width. The normalization uncertainty (3.5% from the minimum-bias cross section and 5.3% from the branching ratio uncertainties) is not shown. Theoretical prediction from GM-VFNS [6] is also shown.

the top panels of Fig. 4. In the bottom panels of the same figure, the ratios of the D_s^+ cross section to the D^0 and D^+ ones are displayed. In the evaluation of the systematic uncertainties on the D meson ratios, the sources of correlated and uncorrelated systematic effects were treated separately. In particular, the contributions of the yield extraction, cut efficiency and PID selection were considered as uncorrelated and summed in quadrature. The systematic uncertainty on the B feed-down subtraction, being completely correlated, was estimated from the spread of the cross section ratios obtained by varying the factorization and renormalization scales and the heavy quark mass in FONLL coherently for all mesons. The uncertainty on the tracking efficiency cancels completely in the ratios between production cross sections of mesons reconstructed from three-body decay channels (D^+, D^{*+} and D_s^+), while a 4% systematic error was considered in the ratios involving the D^0 mesons, which are reconstructed from a two-particle final state. The D_s^+/D^0 and D_s^+/D^+ ratios were corrected for the different value of pp

Table 3: Production cross section in $|y| < 0.5$ for prompt D_s^+ mesons in pp collisions at $\sqrt{s} = 7$ TeV, in $p_{\rm T}$ intervals. The normalization uncertainty (3.5% from the minimum-bias cross section and 5.3% from the branching ratio) is not included in the systematic uncertainties reported in the table.

$p_{\rm T}$ interval (GeV/c)	$\langle p_{\rm T} \rangle$ (GeV/c)	$d\sigma/dp_{\rm T}|_{|y|<0.5}$ $\pm$ stat. $\pm$ syst. (μb GeV^{-1}c)
2–4	2.7 ± 0.4	$19.8 \pm 6.1^{+5.7}_{-6.7}$
4–6	4.7 ± 0.1	$5.04 \pm 1.03^{+1.3}_{-1.5}$
6–8	6.8 ± 0.1	$1.01 \pm 0.28^{+0.26}_{-0.30}$
8–12	9.4 ± 0.1	$0.28 \pm 0.06^{+0.08}_{-0.09}$

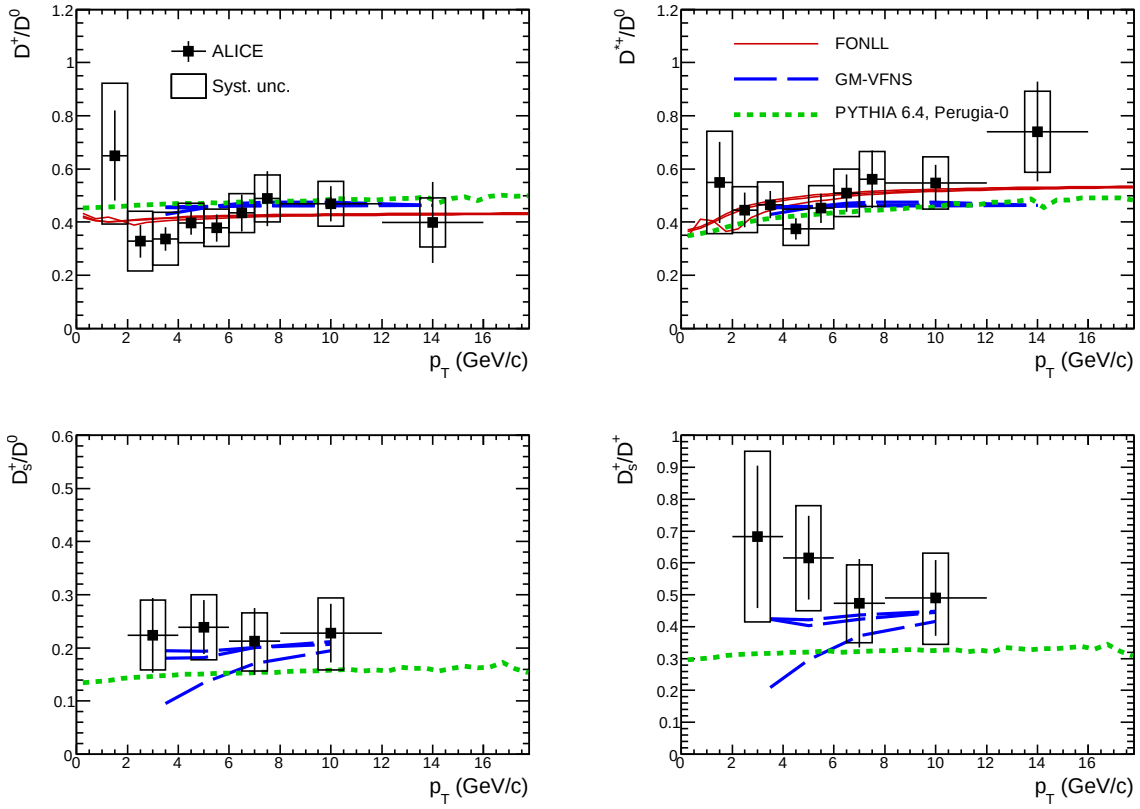

Figure 4: Ratios of D meson production cross sections as a function of p_{T}. Predictions from FONLL, GM-VFNS and PYTHIA 6.4.21 with the Perugia-0 tune are also shown. For FONLL and GM-VFNS three sets of curves are shown, corresponding to the central, upper and lower values of the theoretical uncertainty band for the cross section of the D meson species involved in the ratio.

minimum-bias cross section used in [3] and in this analysis [2].

The predictions from FONLL (only for D^0, D^+ and D^{*+} mesons), GM-VFNS, and the PYTHIA 6.4.21 event generator with the Perugia-0 tune are also shown. For all these model predictions, D mesons in the rapidity range $|y| < 0.5$ were considered. In PYTHIA, the default configuration of the Perugia-0 tune for charm hadronization was used.

The $\mathrm{D}^+/\mathrm{D}^0$ and $\mathrm{D}^{*+}/\mathrm{D}^0$ ratios are determined in PYTHIA by an input parameter, PARJ(13), that defines the probability that a charm or heavier meson has spin 1. In the Perugia-0 tune, this parameter is set to 0.54 from the measured fractions $\mathrm{P_v}$ of heavy flavour mesons produced in vector state, see e.g. [4, 23]. This setting results in an enhancement of the $\mathrm{D}^+/\mathrm{D}^0$ and a reduction of the $\mathrm{D}^{*+}/\mathrm{D}^0$ ratios with respect to those obtained with the default value, PARJ(13)=0.75, based on spin counting.

The $\mathrm{D_s^+}/\mathrm{D}^0$ and $\mathrm{D_s^+}/\mathrm{D}^+$ ratios in PYTHIA are governed by another input parameter, PARJ(2), that defines the s/u (s/d) quark suppression factor in the fragmentation process. In the Perugia-0 tune, PARJ(2) is set to 0.2, which gives rise to a reduced abundance of $\mathrm{D_s^+}$ mesons with respect to the default value of 0.3. With this parameter adjustment, PYTHIA with the Perugia-0 tune reproduces reasonably well the value and p_{T} shapes of the measured ratios involving D^0, D^+ and D^{*+}, while it slightly underestimates the abundance of $\mathrm{D_s^+}$ mesons. The fact that PYTHIA with Perugia-0 tune underestimates the strangeness production was already observed at the LHC in the light flavour sector [54, 55].

[2] The preliminary pp minimum-bias cross section value of 62.5 mb, used in [3], was updated to 62.2 mb.

In the Perugia 2011 tune [56], PARJ(13) is set to the same value (0.54) as in the Perugia-0 tune, while a lower value of the strangeness suppression factor, PARJ(2)=0.19, is used. This results in the same values of the Perugia-0 tune for the D^+/D^0 and D^{*+}/D^0 ratios, and in slightly lower values for the D_s^+/D^0 and D_s^+/D^+ ratios.

The ratios of the FONLL and GM-VFNS predictions were computed assuming the perturbative uncertainty to be fully correlated among the D meson species, i.e. using the same scales for the cross sections at the numerator and at the denominator. Thus, the perturbative uncertainty cancels almost completely in the ratio, as it can be seen in Fig. 4 where for both FONLL and GM-VFNS three sets of curves are shown for each D meson ratio, corresponding to the central, upper and lower values of the theoretical uncertainty band. The predictions from FONLL and GM-VFNS agree within uncertainties with the measured particle ratios. Indeed, in FONLL and GM-VFNS, the relative abundances of the various D meson species are not predicted by the theory: the fragmentation fractions $f(c \to D)$ are taken from the experimental measurements. On the other hand, in both the pQCD calculations, the p_T dependence of the ratios of the D meson production cross sections arises from the different fragmentation functions used to model the transfer of energy from the charm quark to a specific D meson species [22, 57, 58] and from the different contribution from decays of higher excited states. The parton fragmentation models used in the calculations provide an adequate description of the measured data. The measured D_s^+/D^0 and D_s^+/D^+ ratios do not show a significant p_T dependence within the experimental uncertainties, thus suggesting a small difference between the fragmentation functions of c quarks to strange and non-strange mesons. A higher statistics data sample would be needed to conclude on a possible p_T dependence of the ratios of strange to non-strange D meson cross sections.

6.2 p_T-integrated D_s^+ cross section and D meson ratios

The visible cross section of prompt D_s^+ mesons, obtained by integrating the p_T-differential cross section in the measured p_T range ($2 < p_T < 12$ GeV/c), is

$$\sigma_{\rm vis}^{D_s^+} = 53 \pm 12(\text{stat.})^{+13}_{-15}(\text{syst.}) \pm 2(\text{lumi.}) \pm 3(\text{BR})\ \mu\text{b}.$$

The production cross section per unit of rapidity, $d\sigma/dy$, at mid-rapidity was computed by extrapolating the visible cross section to the full p_T range. The extrapolation factor was extracted from the FONLL-based predictions for the D_s^+ p_T-differential cross section described in Section 5. The extrapolation factor was taken as the ratio between the total D_s^+ production cross section in $|y| < 0.5$ and the cross section integrated in $|y| < 0.5$ and in the p_T range where the experimental measurement is performed. In particular, the central value of the extrapolation factor was computed from the prediction based on the p_T-differential cross section of c quarks from FONLL, the fractions $f(c \to D)$ from ALEPH [17], and the fragmentation functions from [51] with $r = 0.1$. The uncertainty on the extrapolation factor was obtained as a quadratic sum of the uncertainties from charm mass and perturbative scales, varied in the ranges described above, and from the CTEQ6.6 parton distribution functions [59]. Furthermore, to account for the uncertainty on the D_s^+ fragmentation function, the extrapolation factors and their uncertainties were also computed using the FONLL predictions for D^0, D^+ and D^{*+} mesons and the envelope of the results was assigned as systematic uncertainty. The resulting value for the extrapolation factor is $2.23^{+0.71}_{-0.65}$. The prompt D_s^+ production cross section per unit of rapidity in $|y| < 0.5$ is then

$$d\sigma^{D_s^+}/dy = 118 \pm 28(\text{stat.})^{+28}_{-34}(\text{syst.}) \pm 4(\text{lumi.}) \pm 7(\text{BR})^{+38}_{-35}(\text{extr.})\ \mu\text{b}.$$

The D meson production ratios were computed from the cross sections per unit of rapidity, $d\sigma/dy$. The corresponding values for D^0, D^+ and D^{*+} from [3] were corrected to account for the updated value of the pp minimum-bias cross section. The systematic uncertainties on the ratios were computed taking into account the correlated and uncorrelated sources as described above. The resulting values are reported in Table 4 and shown in the left-hand panel of Fig. 5 together with the results by other

Table 4: Ratios of the measured production cross section for prompt D mesons in $p_{\rm T} > 0$ and $|y| < 0.5$ in pp collisions at $\sqrt{s} = 7$ TeV.

	Ratio $\pm$ (stat.) $\pm$ (syst.) $\pm$ (BR)
$\rm D^+/D^0$	0.48 $\pm$ 0.07 $\pm$ 0.11 $\pm$ 0.01
$\rm D^{*+}/D^0$	0.48 $\pm$ 0.07 $\pm$ 0.08 $\pm$ 0.01
$\rm D_s^+/D^0$	0.23 $\pm$ 0.06 $\pm$ 0.08 $\pm$ 0.01
$\rm D_s^+/D^+$	0.48 $\pm$ 0.13 $\pm$ 0.17 $\pm$ 0.03

experiments that measured prompt charm production: LHCb [11], $\rm e^+e^-$ data (taken from the compilation in [60]), and ep data in photoproduction from ZEUS [23] and DIS from H1 [16]. The error bars are the quadratic sum of statistical and systematic uncertainties and do not include the uncertainty on the decay branching ratios, which are common to all experiments. The particle ratios for ZEUS and $\rm e^+e^-$ were computed from the compilation of fragmentation fractions $f(\rm c \to D)$ published in [23] after updating the branching ratios of the considered decay channels to the most recent values [46]. For the ZEUS data, the systematic uncertainties were propagated to the particle ratios by properly taking into account correlated and uncorrelated sources [61]. For the H1 data, the D meson ratios were computed starting from the unconstrained values of $f(\rm c \to D)$ published in [16], taking into account the correlated part of the systematic uncertainty and subtracting from the quoted 'theoretical' uncertainty the contribution due to the decay branching ratio [62]. Also in this case, a correction was applied to account for the updates in the branching ratios of the considered decay channels. The ALICE results are compatible with the other measurements within uncertainties.

The values predicted by PYTHIA 6.4.21 with the Perugia-0 tune are also shown in the figure, as well as those from a canonical implementation of the Statistical Hadronization Model (SHM) [63]. The values from PYTHIA were obtained by integrating the prompt D meson yields in the range $|y| < 0.5$ and $p_{\rm T} > 0$. The SHM provides a good description of the measured hadron yields in heavy-ion collisions at various energies and centralities [64], but it can also be applied to small systems like pp [65] and $\rm e^+e^-$ [66, 67]. The SHM results used for the present comparison were computed for prompt D mesons, assuming a temperature T of 164 MeV and a volume V of 30 ± 10 fm^3. The dependence on temperature of the cross section ratios considered in this analysis is rather small within the few MeV uncertainty on the value of T. To properly reproduce the yield of strange particles in small systems, such as pp and $\rm e^+e^-$, an additional parameter, the fugacity [65], is usually introduced in the partition function to account for the deviation of strange particle yields from their chemical equilibrium values. For the SHM predictions reported here, a value of strangeness fugacity of 0.60 ± 0.04, extrapolated from the results of a fit to particle yields in pp collisions at $\sqrt{s} = 200$ GeV [68], was used. With these parameters, the SHM provides a good description of the measured ratios of D meson cross sections.

The strangeness suppression factor for charm mesons, $\gamma_{\rm s}$, was also evaluated. It is defined as the ratio of the production cross sections of charm-strange mesons ($\rm c\bar{s}$) to that of non-strange charm mesons (average of $\rm c\bar{d}$ and $\rm c\bar{u}$) [3]. Since all $\rm D^{*+}$ and $\rm D^{*0}$ mesons decay into either a $\rm D^0$ or a $\rm D^+$, and all $\rm D_s^{*+}$ decays produce a $\rm D_s^+$ meson [46], the strangeness suppression factor was computed as

$$\gamma_{\rm s} = \frac{2\,{\rm d}\sigma({\rm D_s^+})/{\rm d}y}{{\rm d}\sigma({\rm D^0})/{\rm d}y + {\rm d}\sigma({\rm D^+})/{\rm d}y}. \quad (2)$$

The contribution to $\rm D^0$ and $\rm D^+$ yield from decays of excited charm-strange mesons heavier than $\rm D_s^{*+}$ was neglected.

[3] The same symbol $\gamma_{\rm s}$ is used in the statistical hadronization model to indicate the fugacity, which, as mentioned above, is usually included in the partition function to account for strangeness suppression. However, the two $\gamma_{\rm s}$ are different. Indeed, in the statistical hadronization model, the value of the ratio between strange and non-strange charm mesons is proportional to the fugacity, but not equal to it, due to the different masses of the various D meson species.

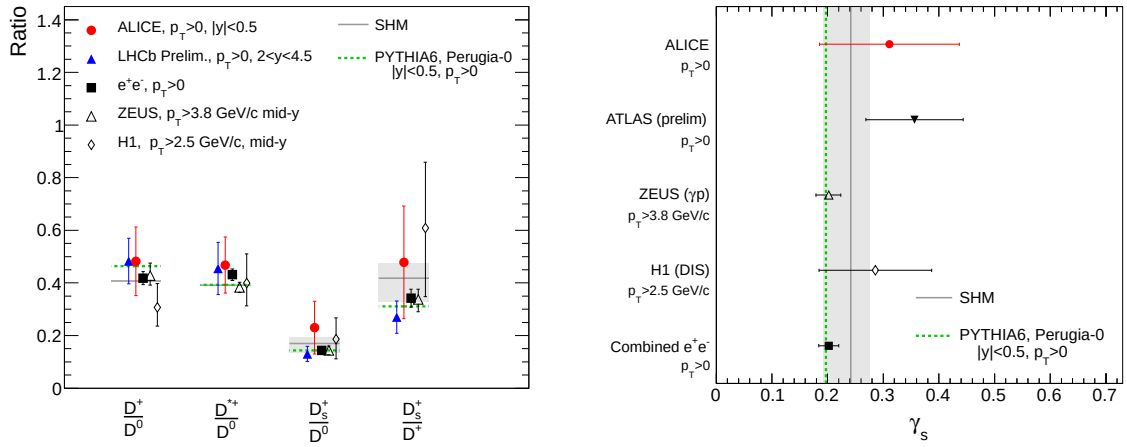

Figure 5: Left: $p_{\rm T}$ integrated ratios of D meson production cross sections compared with other experiments [11, 16, 23, 60]. Error bars are the quadratic sum of statistical and systematic uncertainties, without including the uncertainty on the BR which is common to all experiments. Right: strangeness suppression factor $\gamma_{\rm s}$ compared to measurements by other experiments [12, 16, 23, 60]. Predictions from PYTHIA 6.4.21 with the Perugia-0 tune and from a canonical implementation of the statistical hadronization model (SHM) [63] are also shown. The gray band represents the uncertainty on the SHM predictions due to the uncertainty on the volume and on the strangeness fugacity (see text for details).

The resulting value of $\gamma_{\rm s}$, computed from the $\rm D_s^+$, $\rm D^0$ and $\rm D^+$ cross sections per unit of rapidity ($\rm d\sigma/dy$), is

$$\gamma_{\rm s} = 0.31 \pm 0.08(\text{stat.}) \pm 0.10(\text{syst.}) \pm 0.02(\text{BR}).$$

Charm-strange meson production is suppressed by a factor ≈ 3.3 in the fragmentation of charm quarks. In the right-hand panel of Fig. 5, this result is compared with the $\gamma_{\rm s}$ measurements by other experiments, taken from the compilation in [15], after updating the branching ratios of the considered decay channels to the values in [46]. The preliminary measurement by ATLAS [12] in pp collisions at the LHC, obtained using an equivalent (under the hypothesis of isospin symmetry between u and d quarks) definition of the strangeness suppression factor based on the cross sections of $\rm D_s^+$, $\rm D^+$ and $\rm D^{*+}$ in charm hadronization, is also shown. The error bars are the quadratic sum of statistical and systematic uncertainties and do not include the uncertainty on the decay BR. The values from PYTHIA with the Perugia-0 tune, where $\gamma_{\rm s}$ corresponds to PARJ(2), and the statistical hadronization model described above are also shown for reference. It is also interesting to note that a similar amount of strangeness suppression was reported for beauty mesons by the LHCb Collaboration that measured the ratio of strange B mesons to light neutral B mesons, $f_{\rm s}/f_{\rm d}$, obtaining the value $0.267^{+0.021}_{-0.020}$ [69].

All the $\gamma_{\rm s}$ measurements, performed in different colliding systems and at different centre-of-mass energies are compatible within experimental uncertainties. The current ALICE and ATLAS results at LHC energy in the central rapidity region do not allow one to conclude on a possible lifting of strangeness suppression with increasing collision energy. Furthermore, the $\rm D_s^+/D^0$ ($\rm D_s^+/D^+$) ratios are measured at the LHC both at midrapidity and at forward rapidity, thus allowing to study a possible rapidity dependence of the strangeness suppression in charm hadronization. From the comparison of the ALICE and LHCb results with the current experimental uncertainties (left-hand panel of Fig. 5), it is not possible to draw a firm conclusion on this point.

7 Summary

The inclusive production cross section for prompt D_s^+ meson has been measured in the transverse momentum range $2 < p_T < 12$ GeV/c at central rapidity in pp collisions at $\sqrt{s}$ = 7 TeV. D_s^+ mesons were reconstructed in the hadronic decay channel $D_s^+ \to \phi\pi^+$ with $\phi \to K^-K^+$, and charge conjugates, using the ALICE detector. The measured differential cross section is described within uncertainties by the prediction from the GM-VFNS calculation, which is based on perturbative QCD with the factorization approach. The relative D meson production yields and the strangeness suppression factor, $\gamma_s = 0.31 \pm 0.08(\text{stat.}) \pm 0.10(\text{syst.}) \pm 0.02(\text{BR})$, agree within the present experimental uncertainties with those measured by other experiments for different centre-of-mass energies and colliding systems. More precise measurements are needed to address the possible energy and rapidity dependence of strangeness suppression in charm hadronization.

References

[1] M. Cacciari, M. Greco and P. Nason, JHEP **9805** (1998) 007;
M. Cacciari, S. Frixione and P. Nason, JHEP **0103** (2001) 006.

[2] B.A. Kniehl *et al.*, Phys. Rev. **D77** (2008) 014011;
B.A. Kniehl *et al.*, Phys. Rev. Lett. **96** (2006) 012001.

[3] B. Abelev *et al.* [ALICE Collaboration], JHEP **1201** (2012) 128

[4] B. I. Abelev *et al.* [ALICE Collaboration], arXiv:1205.4007 [hep-ex].

[5] M. Cacciari, S. Frixione, N. Houdeau, M. L. Mangano, P. Nason and G. Ridolfi, CERN-PH-TH/2011-227, arXiv:1205.6344 [hep-ph].

[6] B. A. Kniehl, G. Kramer, I. Schienbein and H. Spiesberger, DESY 12-013, MZ-TH/12-07, LPSC 12019, arXiv:1202.0439 [hep-ph].

[7] D. Acosta *et al.* [CDF II Collaboration], Phys. Rev. Lett. **91** (2003) 241804.

[8] M. Cacciari and P. Nason, JHEP **0309** (2003) 006.

[9] A. Adare *et al.* [PHENIX Collaboration], Phys. Rev. Lett. **97** (2006) 252002.

[10] B.I. Abelev *et al.* [STAR Collaboration], Phys. Rev. Lett. **98** (2007) 192301.

[11] LHCb Collaboration, LHCb-CONF-2010-013 (2010).

[12] ATLAS Collaboration, ATLAS-CONF-2011-017 (2011).

[13] RAaij *et al.* [LHCb Collaboration], Phys. Lett. **713** (2012) 186.

[14] E. Norrbin and T. Sjostrand, Eur. Phys. J. C **17** (2000) 137 [hep-ph/0005110].

[15] S. Chekanov *et al.* [ZEUS Collaboration], JHEP **0707** (2007) 074.

[16] A. Aktas *et al.* [H1 Collaboration], Eur. Phys. J. C **38** (2005) 447.

[17] R. Barate *et al.* [ALEPH Collaboration], Eur. Phys. J. C **16** (2000) 597.

[18] P. Abreu *et al.* [DELPHI Collaboration], Eur. Phys. J. C **12** (2000) 209.

[19] G. Alexander *et al.* [OPAL Collaboration], Z. Phys. C **72** (1996) 1.

[20] D. Bortoletto *et al.* [CLEO Collaboration], Phys. Rev. D **37** (1988) 1719; [Erratum-ibid. D **39** (1989) 1471];
R. A. Briere *et al.* [CLEO Collaboration], Phys. Rev. D **62** (2000) 072003;
M. Artuso *et al.* [CLEO Collaboration], Phys. Rev. D **70** (2004) 112001.

[21] H. Albrecht *et al.* [ARGUS Collaboration], Z. Phys. C **52** (1991) 353;
H. Albrecht *et al.* [ARGUS Collaboration], Z. Phys. C **54** (1992) 1.

[22] B. A. Kniehl and G. Kramer, Phys. Rev. D **74** (2006) 037502.

[23] S. Chekanov *et al.* [ZEUS Collaboration], Eur.Phys.J C 44 (2005) 351.
[24] E. V. Shuryak, Phys. Rept. 61 (1980) 71; F. Karsch, J. Phys. Conf. Ser. **46** (2006) 122; R. Stock, In *Landolt-Boernstein I 21A: Elementary particles* 7, arXiv:0807.1610 [nucl-ex].
[25] Y. L. Dokshitzer, D. E. Kharzeev, Phys. Lett. **B519** (2001) 199.
[26] N. Armesto, A. Dainese, C. A. Salgado and U. A. Wiedemann, Phys. Rev. **D71** (2005) 054027.
[27] B. Abelev *et al.* [ALICE Collaboration], arXiv:1203.2160 [nucl-ex].
[28] F. Antinori *et al.* [NA57 Collaboration], J. Phys. G G **32** (2006) 427.
[29] B. I. Abelev *et al.* [STAR Collaboration], Phys. Rev. C **79** (2009) 034909.
[30] G. Agakishiev *et al.* [STAR Collaboration], Phys. Rev. Lett. **108** (2012) 072301.
[31] B. Hippolyte [for the ALICE Collaboration], arXiv:1112.5803 [nucl-ex].
[32] I. Kuznetsova and J. Rafelski, Eur.Phys.J. **C51** (2007) 113-133.
[33] M. He, R. J. Fries and R. Rapp, arXiv:1204.4442 [nucl-th].
[34] A. Andronic, P. Braun-Munzinger, K. Redlich and J. Stachel, Phys. Lett. B **571** (2003) 36.
[35] J. Adams *et al.* [STAR Collaboration], Phys. Rev. Lett. **95** (2005) 122301.
[36] J. Adams *et al.* [STAR Collaboration], Phys. Rev. Lett. **92** (2004) 52302.
[37] S.S. Adler *et al.* [PHENIX Collaboration], Phys. Rev. C. **69** (2004) 034909.
[38] K. Aamodt *et al.* [ALICE Collaboration], JINST **3** (2008) S08002.
[39] K. Aamodt *et al.* [ALICE Collaboration], JINST **5** (2010) P03003.
[40] J. Alme *et al.*, Nucl. Instrum. Meth. **A622** (2010) 316.
[41] K. Aamodt *et al.* [ALICE Collaboration], Eur. Phys. J. C **71** (2011) 1655.
[42] M. Gagliardi *et al.* [ALICE Collaboration], arXiv:1109.5369 [hep-ex].
[43] B. Abelev *et al.* [ALICE Collaboration], "Measurement of inelastic, single and double diffraction cross sections in proton-proton collisions at LHC with ALICE", in preparation.
[44] T. Sjöstrand, S. Mrenna and P. Z. Skands, JHEP **0605** (2006) 026.
[45] P.Z. Skands, arXiv:0905.3418 (2009).
[46] J. Beringer *et al.*, [Particle Data Group], Phys. Rev. **D86** (2012) 010001.
[47] K. Oyama for the ALICE collaboration, to appear on the Proceedings of the LHC Lumi Days 2012.
[48] S. van der Meer, ISR-PO/68-31, KEK68-64.
[49] R. Brun *et al.*, CERN Program Library Long Write-up, W5013, GEANT Detector Description and Simulation Tool (1994).
[50] D.J. Lange, Nucl. Instrum. Methods **A462** (2001) 152.
[51] E. Braaten, K. -m. Cheung, S. Fleming and T. C. Yuan, Phys. Rev. D **51** (1995) 4819.
[52] M. Cacciari and P. Nason, JHEP **0309** (2003) 006.
[53] B.A. Kniehl *et al.*, Phys. Rev. Lett. **96** (2006) 012001.
[54] K. Aamodt *et al.* [ALICE Collaboration], Eur. Phys. J. C **71** (2011) 1594.
[55] V. Khachatryan *et al.* [CMS Collaboration], JHEP **1105** (2011) 064.
[56] P. Z. Skands, Phys. Rev. D **82** (2010) 074018.
[57] M. Cacciari and P. Nason, JHEP **0309** (2003) 006.
[58] T. Kneesch, B. A. Kniehl, G. Kramer and I. Schienbein, Nucl. Phys. B **799** (2008) 34.
[59] P.M. Nadolsky *et al.*, Phys. Rev. **D78** (2008) 013004.
[60] L. Gladilin, arXiv:hep-ex/9912064 (1999).
[61] Private communication with Zeus Collaboration.
[62] Private communication with H1 Collaboration.
[63] A. Andronic, F. Beutler, P. Braun-Munzinger, K. Redlich and J. Stachel, Phys. Lett. B **678** (2009)

350; and private communication.
[64] A. Andronic, P. Braun-Munzinger and J. Stachel, Phys. Lett. B **673** (2009) 142
[65] I. Kraus, J. Cleymans, H. Oeschler and K. Redlich, Phys. Rev. C **79** (2009) 014901.
[66] F. Becattini, Z. Phys. C **69** (1996) 485.
[67] F. Becattini, J. Phys. G G **23** (1997) 1933
[68] B. I. Abelev *et al.* [STAR Collaboration], Phys. Rev. C **79** (2009) 034909.
[69] R. Aaij *et al.* [LHCb Collaboration], Phys. Rev. D **85** (2012) 032008.

8 Acknowledgements

The ALICE collaboration would like to thank all its engineers and technicians for their invaluable contributions to the construction of the experiment and the CERN accelerator teams for the outstanding performance of the LHC complex. The ALICE Collaboration would like to thank M. Cacciari and H. Spiesberger for providing pQCD predictions that are used for the feed-down correction and for comparison to the measured data. The ALICE Collaboration would like to thank the Zeus and H1 collaborations, and in particular L. Gladilin and K. Krueger, for providing updated values of the branching fractions and D meson ratios.
The ALICE collaboration acknowledges the following funding agencies for their support in building and running the ALICE detector:
Calouste Gulbenkian Foundation from Lisbon and Swiss Fonds Kidagan, Armenia;
Conselho Nacional de Desenvolvimento Científico e Tecnológico (CNPq), Financiadora de Estudos e Projetos (FINEP), Fundação de Amparo à Pesquisa do Estado de São Paulo (FAPESP);
National Natural Science Foundation of China (NSFC), the Chinese Ministry of Education (CMOE) and the Ministry of Science and Technology of China (MSTC);
Ministry of Education and Youth of the Czech Republic;
Danish Natural Science Research Council, the Carlsberg Foundation and the Danish National Research Foundation;
The European Research Council under the European Community's Seventh Framework Programme;
Helsinki Institute of Physics and the Academy of Finland;
French CNRS-IN2P3, the 'Region Pays de Loire', 'Region Alsace', 'Region Auvergne' and CEA, France;
German BMBF and the Helmholtz Association;
General Secretariat for Research and Technology, Ministry of Development, Greece;
Hungarian OTKA and National Office for Research and Technology (NKTH);
Department of Atomic Energy and Department of Science and Technology of the Government of India;
Istituto Nazionale di Fisica Nucleare (INFN) of Italy;
MEXT Grant-in-Aid for Specially Promoted Research, Japan;
Joint Institute for Nuclear Research, Dubna;
National Research Foundation of Korea (NRF);
CONACYT, DGAPA, México, ALFA-EC and the HELEN Program (High-Energy physics Latin-American–European Network);
Stichting voor Fundamenteel Onderzoek der Materie (FOM) and the Nederlandse Organisatie voor Wetenschappelijk Onderzoek (NWO), Netherlands;
Research Council of Norway (NFR);
Polish Ministry of Science and Higher Education;
National Authority for Scientific Research - NASR (Autoritatea Naţională pentru Cercetare Ştiinţifică - ANCS);
Federal Agency of Science of the Ministry of Education and Science of Russian Federation, International Science and Technology Center, Russian Academy of Sciences, Russian Federal Agency of Atomic En-

ergy, Russian Federal Agency for Science and Innovations and CERN-INTAS;
Ministry of Education of Slovakia;
Department of Science and Technology, South Africa;
CIEMAT, EELA, Ministerio de Educación y Ciencia of Spain, Xunta de Galicia (Consellería de Educación), CEADEN, Cubaenergía, Cuba, and IAEA (International Atomic Energy Agency);
Swedish Research Council (VR) and Knut & Alice Wallenberg Foundation (KAW);
Ukraine Ministry of Education and Science;
United Kingdom Science and Technology Facilities Council (STFC);
The United States Department of Energy, the United States National Science Foundation, the State of Texas, and the State of Ohio.

A The ALICE Collaboration

B. Abelev[68] , J. Adam[34] , D. Adamová[73] , A.M. Adare[120] , M.M. Aggarwal[77] , G. Aglieri Rinella[30] , A.G. Agocs[60] , A. Agostinelli[19] , S. Aguilar Salazar[56] , Z. Ahammed[116] , N. Ahmad[14] , A. Ahmad Masoodi[14] , S.A. Ahn[62] , S.U. Ahn[37] , A. Akindinov[46] , D. Aleksandrov[88] , B. Alessandro[94] , R. Alfaro Molina[56] , A. Alici[97 ,10] , A. Alkin[2] , E. Almaráz Aviña[56] , J. Alme[32] , T. Alt[36] , V. Altini[28] , S. Altinpinar[15] , I. Altsybeev[117] , C. Andrei[70] , A. Andronic[85] , V. Anguelov[82] , J. Anielski[54] , C. Anson[16] , T. Antičić[86] , F. Antinori[93] , P. Antonioli[97] , L. Aphecetche[102] , H. Appelshäuser[52] , N. Arbor[64] , S. Arcelli[19] , A. Arend[52] , N. Armesto[13] , R. Arnaldi[94] , T. Aronsson[120] , I.C. Arsene[85] , M. Arslandok[52] , A. Asryan[117] , A. Augustinus[30] , R. Averbeck[85] , T.C. Awes[74] , J. Äystö[38] , M.D. Azmi[14 ,79] , M. Bach[36] , A. Badalà[99] , Y.W. Baek[63 ,37] , R. Bailhache[52] , R. Bala[94] , R. Baldini Ferroli[10] , A. Baldisseri[12] , A. Baldit[63] , F. Baltasar Dos Santos Pedrosa[30] , J. Bán[47] , R.C. Baral[48] , R. Barbera[25] , F. Barile[28] , G.G. Barnaföldi[60] , L.S. Barnby[90] , V. Barret[63] , J. Bartke[104] , M. Basile[19] , N. Bastid[63] , S. Basu[116] , B. Bathen[54] , G. Batigne[102] , B. Batyunya[59] , C. Baumann[52] , I.G. Bearden[71] , H. Beck[52] , I. Belikov[58] , F. Bellini[19] , R. Bellwied[110] , E. Belmont-Moreno[56] , G. Bencedi[60] , S. Beole[23] , I. Berceanu[70] , A. Bercuci[70] , Y. Berdnikov[75] , D. Berenyi[60] , A.A.E. Bergognon[102] , D. Berzano[94] , L. Betev[30] , A. Bhasin[80] , A.K. Bhati[77] , J. Bhom[114] , L. Bianchi[23] , N. Bianchi[65] , C. Bianchin[20] , J. Bielčík[34] , J. Bielčíková[73] , A. Bilandzic[72 ,71] , S. Bjelogrlic[45] , F. Blanco[8] , F. Blanco[110] , D. Blau[88] , C. Blume[52] , M. Boccioli[30] , N. Bock[16] , S. Böttger[51] , A. Bogdanov[69] , H. Bøggild[71] , M. Bogolyubsky[43] , L. Boldizsár[60] , M. Bombara[35] , J. Book[52] , H. Borel[12] , A. Borissov[119] , S. Bose[89] , F. Bossú[23] , M. Botje[72] , E. Botta[23] , B. Boyer[42] , E. Braidot[67] , P. Braun-Munzinger[85] , M. Bregant[102] , T. Breitner[51] , T.A. Browning[83] , M. Broz[33] , R. Brun[30] , E. Bruna[23 ,94] , G.E. Bruno[28] , D. Budnikov[87] , H. Buesching[52] , S. Bufalino[23 ,94] , O. Busch[82] , Z. Buthelezi[79] , D. Caballero Orduna[120] , D. Caffarri[20 ,93] , X. Cai[5] , H. Caines[120] , E. Calvo Villar[91] , P. Camerini[21] , V. Canoa Roman[9] , G. Cara Romeo[97] , F. Carena[30] , W. Carena[30] , N. Carlin Filho[107] , F. Carminati[30] , A. Casanova Díaz[65] , J. Castillo Castellanos[12] , J.F. Castillo Hernandez[85] , E.A.R. Casula[22] , V. Catanescu[70] , C. Cavicchioli[30] , C. Ceballos Sanchez[7] , J. Cepila[34] , P. Cerello[94] , B. Chang[38 ,123] , S. Chapeland[30] , J.L. Charvet[12] , S. Chattopadhyay[116] , S. Chattopadhyay[89] , I. Chawla[77] , M. Cherney[76] , C. Cheshkov[30 ,109] , B. Cheynis[109] , V. Chibante Barroso[30] , D.D. Chinellato[108] , P. Chochula[30] , M. Chojnacki[45] , S. Choudhury[116] , P. Christakoglou[72] , C.H. Christensen[71] , P. Christiansen[29] , T. Chujo[114] , S.U. Chung[84] , C. Cicalo[96] , L. Cifarelli[19 ,30 ,10] , F. Cindolo[97] , J. Cleymans[79] , F. Coccetti[10] , F. Colamaria[28] , D. Colella[28] , G. Conesa Balbastre[64] , Z. Conesa del Valle[30] , P. Constantin[82] , G. Contin[21] , J.G. Contreras[9] , T.M. Cormier[119] , Y. Corrales Morales[23] , P. Cortese[27] , I. Cortés Maldonado[1] , M.R. Cosentino[67] , F. Costa[30] , M.E. Cotallo[8] , E. Crescio[9] , P. Crochet[63] , E. Cruz Alaniz[56] , E. Cuautle[55] , L. Cunqueiro[65] , A. Dainese[20 ,93] , H.H. Dalsgaard[71] , A. Danu[50] , I. Das[42] , D. Das[89] , K. Das[89] , S. Dash[40] , A. Dash[108] , S. De[116] , G.O.V. de Barros[107] , A. De Caro[26 ,10] , G. de Cataldo[98] , J. de Cuveland[36] , A. De Falco[22] , D. De Gruttola[26] , H. Delagrange[102] , A. Deloff[100] , V. Demanov[87] , N. De Marco[94] , E. Dénes[60] , S. De Pasquale[26] , A. Deppman[107] , G. D Erasmo[28] , R. de Rooij[45] , M.A. Diaz Corchero[8] , D. Di Bari[28] , T. Dietel[54] , C. Di Giglio[28] , S. Di Liberto[95] , A. Di Mauro[30] , P. Di Nezza[65] , R. Divià[30] , Ø. Djuvsland[15] , A. Dobrin[119 ,29] , T. Dobrowolski[100] , I. Domínguez[55] , B. Dönigus[85] , O. Dordic[18] , O. Driga[102] , A.K. Dubey[116] , A. Dubla[45] , L. Ducroux[109] , P. Dupieux[63] , A.K. Dutta Majumdar[89] , M.R. Dutta Majumdar[116] , D. Elia[98] , D. Emschermann[54] , H. Engel[51] , B. Erazmus[102] , H.A. Erdal[32] , B. Espagnon[42] , M. Estienne[102] , S. Esumi[114] , D. Evans[90] , G. Eyyubova[18] , D. Fabris[20 ,93] , J. Faivre[64] , D. Falchieri[19] , A. Fantoni[65] , M. Fasel[85] , R. Fearick[79] , A. Fedunov[59] , D. Fehlker[15] , L. Feldkamp[54] , D. Felea[50] , B. Fenton-Olsen[67] , G. Feofilov[117] , A. Fernández Téllez[1] , A. Ferretti[23] , R. Ferretti[27] , A. Festanti[20] , J. Figiel[104] , M.A.S. Figueredo[107] , S. Filchagin[87] , D. Finogeev[44] , F.M. Fionda[28] , E.M. Fiore[28] , M. Floris[30] , S. Foertsch[79] , P. Foka[85] , S. Fokin[88] , E. Fragiacomo[92] , A. Francescon[30 ,20] , U. Frankenfeld[85] , U. Fuchs[30] , C. Furget[64] , M. Fusco Girard[26] , J.J. Gaardhøje[71] , M. Gagliardi[23] , A. Gago[91] , M. Gallio[23] , D.R. Gangadharan[16] , P. Ganoti[74] , C. Garabatos[85] , E. Garcia-Solis[11] , I. Garishvili[68] , J. Gerhard[36] , M. Germain[102] , C. Geuna[12] , M. Gheata[50 ,30] , A. Gheata[30] , B. Ghidini[28] , P. Ghosh[116] , P. Gianotti[65] , M.R. Girard[118] , P. Giubellino[30] , E. Gladysz-Dziadus[104] , P. Glässel[82] , R. Gomez[106] , E.G. Ferreiro[13] , L.H. González-Trueba[56] , P. González-Zamora[8] , S. Gorbunov[36] , A. Goswami[81] , S. Gotovac[103] , V. Grabski[56] , L.K. Graczykowski[118] , R. Grajcarek[82] , A. Grelli[45] , C. Grigoras[30] , A. Grigoras[30] , V. Grigoriev[69] , S. Grigoryan[59] , A. Grigoryan[121] , B. Grinyov[2] , N. Grion[92] , P. Gros[29] , J.F. Grosse-Oetringhaus[30] , J.-Y. Grossiord[109] , R. Grosso[30] , F. Guber[44] , R. Guernane[64] , C. Guerra Gutierrez[91] , B. Guerzoni[19] , M. Guilbaud[109] , K. Gulbrandsen[71] , T. Gunji[113] , R. Gupta[80] , A. Gupta[80] , H. Gutbrod[85] , Ø. Haaland[15] , C. Hadjidakis[42] , M. Haiduc[50] , H. Hamagaki[113] , G. Hamar[60] , B.H. Han[17] , L.D. Hanratty[90] , A. Hansen[71] , Z. Harmanová-Tóthová[35] , J.W. Harris[120] , M. Hartig[52] , D. Hasegan[50] , D. Hatzifotiadou[97] , A. Hayrapetyan[30 ,121] , S.T. Heckel[52] , M. Heide[54] , H. Helstrup[32] , A. Herghelegiu[70] , G. Herrera Corral[9] , N. Herrmann[82] , B.A. Hess[115] , K.F. Hetland[32] , B. Hicks[120] , P.T. Hille[120] , B. Hippolyte[58] , T. Horaguchi[114] ,

Y. Hori[113], P. Hristov[30], I. Hřivnáčová[42], M. Huang[15], T.J. Humanic[16], D.S. Hwang[17], R. Ichou[63], R. Ilkaev[87], I. Ilkiv[100], M. Inaba[114], E. Incani[22], G.M. Innocenti[23], P.G. Innocenti[30], M. Ippolitov[88], M. Irfan[14], C. Ivan[85], M. Ivanov[85], A. Ivanov[117], V. Ivanov[75], O. Ivanytskyi[2], P. M. Jacobs[67], H.J. Jang[62], R. Janik[33], M.A. Janik[118], P.H.S.Y. Jayarathna[110], S. Jena[40], D.M. Jha[119], R.T. Jimenez Bustamante[55], L. Jirden[30], P.G. Jones[90], H. Jung[37], A. Jusko[90], A.B. Kaidalov[46], V. Kakoyan[121], S. Kalcher[36], P. Kaliňák[47], T. Kalliokoski[38], A. Kalweit[53,30], J.H. Kang[123], V. Kaplin[69], A. Karasu Uysal[30,122], O. Karavichev[44], T. Karavicheva[44], E. Karpechev[44], A. Kazantsev[88], U. Kebschull[51], R. Keidel[124], P. Khan[89], M.M. Khan[14], S.A. Khan[116], A. Khanzadeev[75], Y. Kharlov[43], B. Kileng[32], M.Kim[37], D.J. Kim[38], D.W. Kim[37], J.H. Kim[17], J.S. Kim[37], T. Kim[123], M. Kim[123], S.H. Kim[37], S. Kim[17], B. Kim[123], S. Kirsch[36], I. Kisel[36], S. Kiselev[46], A. Kisiel[118], J.L. Klay[4], J. Klein[82], C. Klein-Bösing[54], M. Kliemant[52], A. Kluge[30], M.L. Knichel[85], A.G. Knospe[105], K. Koch[82], M.K. Köhler[85], T. Kollegger[36], A. Kolojvari[117], V. Kondratiev[117], N. Kondratyeva[69], A. Konevskikh[44], A. Korneev[87], R. Kour[90], M. Kowalski[104], S. Kox[64], G. Koyithatta Meethaleveedu[40], J. Kral[38], I. Králik[47], F. Kramer[52], I. Kraus[85], T. Krawutschke[82,31], M. Krelina[34], M. Kretz[36], M. Krivda[90,47], F. Krizek[38], M. Krus[34], E. Kryshen[75], M. Krzewicki[85], Y. Kucheriaev[88], T. Kugathasan[30], C. Kuhn[58], P.G. Kuijer[72], I. Kulakov[52], J. Kumar[40], P. Kurashvili[100], A.B. Kurepin[44], A. Kurepin[44], A. Kuryakin[87], S. Kushpil[73], V. Kushpil[73], H. Kvaerno[18], M.J. Kweon[82], Y. Kwon[123], P. Ladrón de Guevara[55], I. Lakomov[42], R. Langoy[15], S.L. La Pointe[45], C. Lara[51], A. Lardeux[102], P. La Rocca[25], C. Lazzeroni[90], R. Lea[21], Y. Le Bornec[42], M. Lechman[30], K.S. Lee[37], G.R. Lee[90], S.C. Lee[37], F. Lefèvre[102], J. Lehnert[52], L. Leistam[30], M. Lenhardt[85], V. Lenti[98], H. León[56], M. Leoncino[94], I. León Monzón[106], H. León Vargas[52], P. Lévai[60], J. Lien[15], R. Lietava[90], S. Lindal[18], V. Lindenstruth[36], C. Lippmann[85,30], M.A. Lisa[16], L. Liu[15], V.R. Loggins[119], V. Loginov[69], S. Lohn[30], D. Lohner[82], C. Loizides[67], K.K. Loo[38], X. Lopez[63], E. López Torres[7], G. Løvhøiden[18], X.-G. Lu[82], P. Luettig[52], M. Lunardon[20], J. Luo[5], G. Luparello[45], L. Luquin[102], C. Luzzi[30], K. Ma[5], R. Ma[120], D.M. Madagodahettige-Don[110], A. Maevskaya[44], M. Mager[53,30], D.P. Mahapatra[48], A. Maire[82], M. Malaev[75], I. Maldonado Cervantes[55], L. Malinina[59,,i], D. Mal'Kevich[46], P. Malzacher[85], A. Mamonov[87], L. Manceau[94], L. Mangotra[80], V. Manko[88], F. Manso[63], V. Manzari[98], Y. Mao[5], M. Marchisone[63,23], J. Mareš[49], G.V. Margagliotti[21,92], A. Margotti[97], A. Marín[85], C.A. Marin Tobon[30], C. Markert[105], I. Martashvili[112], P. Martinengo[30], M.I. Martínez[1], A. Martínez Davalos[56], G. Martínez García[102], Y. Martynov[2], A. Mas[102], S. Masciocchi[85], M. Masera[23], A. Masoni[96], L. Massacrier[102], A. Mastroserio[28], Z.L. Matthews[90], A. Matyja[104,102], C. Mayer[104], J. Mazer[112], M.A. Mazzoni[95], F. Meddi[24], A. Menchaca-Rocha[56], J. Mercado Pérez[82], M. Meres[33], Y. Miake[114], L. Milano[23], J. Milosevic[18,,ii], A. Mischke[45], A.N. Mishra[81], D. Miśkowiec[85,30], C. Mitu[50], J. Mlynarz[119], B. Mohanty[116], L. Molnar[60,30], L. Montaño Zetina[9], M. Monteno[94], E. Montes[8], T. Moon[123], M. Morando[20], D.A. Moreira De Godoy[107], S. Moretto[20], A. Morsch[30], V. Muccifora[65], E. Mudnic[103], S. Muhuri[116], M. Mukherjee[116], H. Müller[30], M.G. Munhoz[107], L. Musa[30], A. Musso[94], B.K. Nandi[40], R. Nania[97], E. Nappi[98], C. Nattrass[112], N.P. Naumov[87], S. Navin[90], T.K. Nayak[116], S. Nazarenko[87], G. Nazarov[87], A. Nedosekin[46], M. Nicassio[28], M.Niculescu[50,30], B.S. Nielsen[71], T. Niida[114], S. Nikolaev[88], V. Nikolic[86], S. Nikulin[88], V. Nikulin[75], B.S. Nilsen[76], M.S. Nilsson[18], F. Noferini[97,10], P. Nomokonov[59], G. Nooren[45], N. Novitzky[38], A. Nyanin[88], A. Nyatha[40], C. Nygaard[71], J. Nystrand[15], A. Ochirov[117], H. Oeschler[53,30], S. Oh[120], S.K. Oh[37], J. Oleniacz[118], C. Oppedisano[94], A. Ortiz Velasquez[29,55], G. Ortona[23], A. Oskarsson[29], P. Ostrowski[118], J. Otwinowski[85], K. Oyama[82], K. Ozawa[113], Y. Pachmayer[82], M. Pachr[34], F. Padilla[23], P. Pagano[26], G. Paić[55], F. Painke[36], C. Pajares[13], S.K. Pal[116], A. Palaha[90], A. Palmeri[99], V. Papikyan[121], G.S. Pappalardo[99], W.J. Park[85], A. Passfeld[54], B. Pastirčák[47], D.I. Patalakha[43], V. Paticchio[98], A. Pavlinov[119], T. Pawlak[118], T. Peitzmann[45], H. Pereira Da Costa[12], E. Pereira De Oliveira Filho[107], D. Peresunko[88], C.E. Pérez Lara[72], E. Perez Lezama[55], D. Perini[30], D. Perrino[28], W. Peryt[118], A. Pesci[97], V. Peskov[30,55], Y. Pestov[3], V. Petráček[34], M. Petran[34], M. Petris[70], P. Petrov[90], M. Petrovici[70], C. Petta[25], S. Piano[92], A. Piccotti[94], M. Pikna[33], P. Pillot[102], O. Pinazza[30], L. Pinsky[110], N. Pitz[52], D.B. Piyarathna[110], M. Planinic[86], M. Płoskoń[67], J. Pluta[118], T. Pocheptsov[59], S. Pochybova[60], P.L.M. Podesta-Lerma[106], M.G. Poghosyan[30,23], K. Polák[49], B. Polichtchouk[43], A. Pop[70], S. Porteboeuf-Houssais[63], V. Pospíšil[34], B. Potukuchi[80], S.K. Prasad[119], R. Preghenella[97,10], F. Prino[94], C.A. Pruneau[119], I. Pshenichnov[44], S. Puchagin[87], G. Puddu[22], A. Pulvirenti[25], V. Punin[87], M. Putiš[35], J. Putschke[119,120], E. Quercigh[30], H. Qvigstad[18], A. Rachevski[92], A. Rademakers[30], T.S. Räihä[38], J. Rak[38], A. Rakotozafindrabe[12], L. Ramello[27], A. Ramírez Reyes[9], S. Raniwala[81], R. Raniwala[81], S.S. Räsänen[38], B.T. Rascanu[52], D. Rathee[77], K.F. Read[112], J.S. Real[64], K. Redlich[100,57], P. Reichelt[52], M. Reicher[45], R. Renfordt[52], A.R. Reolon[65], A. Reshetin[44], F. Rettig[36], J.-P. Revol[30], K. Reygers[82], L. Riccati[94], R.A. Ricci[66], T. Richert[29], M. Richter[18], P. Riedler[30], W. Riegler[30], F. Riggi[25,99], B. Rodrigues Fernandes Rabacal[30], M. Rodríguez Cahuantzi[1], A. Rodriguez Manso[72], K. Røed[15], D. Rohr[36], D. Röhrich[15], R. Romita[85],

F. Ronchetti[65] , P. Rosnet[63] , S. Rossegger[30] , A. Rossi[30 ,20] , P. Roy[89] , C. Roy[58] , A.J. Rubio Montero[8] , R. Rui[21] , R. Russo[23] , E. Ryabinkin[88] , A. Rybicki[104] , S. Sadovsky[43] , K. Šafařík[30] , R. Sahoo[41] , P.K. Sahu[48] , J. Saini[116] , H. Sakaguchi[39] , S. Sakai[67] , D. Sakata[114] , C.A. Salgado[13] , J. Salzwedel[16] , S. Sambyal[80] , V. Samsonov[75] , X. Sanchez Castro[58] , L. Šándor[47] , A. Sandoval[56] , M. Sano[114] , S. Sano[113] , R. Santo[54] , R. Santoro[98 ,30 ,10] , J. Sarkamo[38] , E. Scapparone[97] , F. Scarlassara[20] , R.P. Scharenberg[83] , C. Schiaua[70] , R. Schicker[82] , H.R. Schmidt[115] , C. Schmidt[85] , S. Schreiner[30] , S. Schuchmann[52] , J. Schukraft[30] , Y. Schutz[30 ,102] , K. Schwarz[85] , K. Schweda[85 ,82] , G. Scioli[19] , E. Scomparin[94] , P.A. Scott[90] , R. Scott[112] , G. Segato[20] , I. Selyuzhenkov[85] , S. Senyukov[27 ,58] , J. Seo[84] , S. Serci[22] , E. Serradilla[8 ,56] , A. Sevcenco[50] , A. Shabetai[102] , G. Shabratova[59] , R. Shahoyan[30] , N. Sharma[77] , S. Sharma[80] , S. Rohni[80] , K. Shigaki[39] , M. Shimomura[114] , K. Shtejer[7] , Y. Sibiriak[88] , M. Siciliano[23] , E. Sicking[30] , S. Siddhanta[96] , T. Siemiarczuk[100] , D. Silvermyr[74] , C. Silvestre[64] , G. Simatovic[55 ,86] , G. Simonetti[30] , R. Singaraju[116] , R. Singh[80] , S. Singha[116] , V. Singhal[116] , T. Sinha[89] , B.C. Sinha[116] , B. Sitar[33] , M. Sitta[27] , T.B. Skaali[18] , K. Skjerdal[15] , R. Smakal[34] , N. Smirnov[120] , R.J.M. Snellings[45] , C. Søgaard[71] , R. Soltz[68] , H. Son[17] , J. Song[84] , M. Song[123] , C. Soos[30] , F. Soramel[20] , I. Sputowska[104] , M. Spyropoulou-Stassinaki[78] , B.K. Srivastava[83] , J. Stachel[82] , I. Stan[50] , I. Stan[50] , G. Stefanek[100] , M. Steinpreis[16] , E. Stenlund[29] , G. Steyn[79] , J.H. Stiller[82] , D. Stocco[102] , M. Stolpovskiy[43] , K. Strabykin[87] , P. Strmen[33] , A.A.P. Suaide[107] , M.A. Subieta Vásquez[23] , T. Sugitate[39] , C. Suire[42] , M. Sukhorukov[87] , R. Sultanov[46] , M. Šumbera[73] , T. Susa[86] , T.J.M. Symons[67] , A. Szanto de Toledo[107] , I. Szarka[33] , A. Szczepankiewicz[104 ,30] , A. Szostak[15] , M. Szymański[118] , J. Takahashi[108] , J.D. Tapia Takaki[42] , A. Tauro[30] , G. Tejeda Muñoz[1] , A. Telesca[30] , C. Terrevoli[28] , J. Thäder[85] , D. Thomas[45] , R. Tieulent[109] , A.R. Timmins[110] , D. Tlusty[34] , A. Toia[36 ,20 ,93] , H. Torii[113] , L. Toscano[94] , V. Trubnikov[2] , D. Truesdale[16] , W.H. Trzaska[38] , T. Tsuji[113] , A. Tumkin[87] , R. Turrisi[93] , T.S. Tveter[18] , J. Ulery[52] , K. Ullaland[15] , J. Ulrich[61 ,51] , A. Uras[109] , J. Urbán[35] , G.M. Urciuoli[95] , G.L. Usai[22] , M. Vajzer[34 ,73] , M. Vala[59 ,47] , L. Valencia Palomo[42] , S. Vallero[82] , P. Vande Vyvre[30] , M. van Leeuwen[45] , L. Vannucci[66] , A. Vargas[1] , R. Varma[40] , M. Vasileiou[78] , A. Vasiliev[88] , V. Vechernin[117] , M. Veldhoen[45] , M. Venaruzzo[21] , E. Vercellin[23] , S. Vergara[1] , R. Vernet[6] , M. Verweij[45] , L. Vickovic[103] , G. Viesti[20] , O. Vikhlyantsev[87] , Z. Vilakazi[79] , O. Villalobos Baillie[90] , Y. Vinogradov[87] , A. Vinogradov[88] , L. Vinogradov[117] , T. Virgili[26] , Y.P. Viyogi[116] , A. Vodopyanov[59] , S. Voloshin[119] , K. Voloshin[46] , G. Volpe[28 ,30] , B. von Haller[30] , D. Vranic[85] , G. Øvrebekk[15] , J. Vrláková[35] , B. Vulpescu[63] , A. Vyushin[87] , V. Wagner[34] , B. Wagner[15] , R. Wan[5] , Y. Wang[5] , M. Wang[5] , D. Wang[5] , Y. Wang[82] , K. Watanabe[114] , M. Weber[110] , J.P. Wessels[30 ,54] , U. Westerhoff[54] , J. Wiechula[115] , J. Wikne[18] , M. Wilde[54] , A. Wilk[54] , G. Wilk[100] , M.C.S. Williams[97] , B. Windelband[82] , L. Xaplanteris Karampatsos[105] , C.G. Yaldo[119] , Y. Yamaguchi[113] , S. Yang[15] , H. Yang[12] , S. Yasnopolskiy[88] , J. Yi[84] , Z. Yin[5] , I.-K. Yoo[84] , J. Yoon[123] , W. Yu[52] , X. Yuan[5] , I. Yushmanov[88] , V. Zaccolo[71] , C. Zach[34] , C. Zampolli[97] , S. Zaporozhets[59] , A. Zarochentsev[117] , P. Závada[49] , N. Zaviyalov[87] , H. Zbroszczyk[118] , P. Zelnicek[51] , I.S. Zgura[50] , M. Zhalov[75] , H. Zhang[5] , X. Zhang[63 ,5] , D. Zhou[5] , Y. Zhou[45] , F. Zhou[5] , J. Zhu[5] , X. Zhu[5] , J. Zhu[5] , A. Zichichi[19 ,10] , A. Zimmermann[82] , G. Zinovjev[2] , Y. Zoccarato[109] , M. Zynovyev[2] , M. Zyzak[52]

Affiliation notes

[i] Also at: M.V.Lomonosov Moscow State University, D.V.Skobeltsyn Institute of Nuclear Physics, Moscow, Russia

[ii] Also at: University of Belgrade, Faculty of Physics and ”Vinča” Institute of Nuclear Sciences, Belgrade, Serbia

Collaboration Institutes

[1] Benemérita Universidad Autónoma de Puebla, Puebla, Mexico

[2] Bogolyubov Institute for Theoretical Physics, Kiev, Ukraine

[3] Budker Institute for Nuclear Physics, Novosibirsk, Russia

[4] California Polytechnic State University, San Luis Obispo, California, United States

[5] Central China Normal University, Wuhan, China

[6] Centre de Calcul de l’IN2P3, Villeurbanne, France

[7] Centro de Aplicaciones Tecnológicas y Desarrollo Nuclear (CEADEN), Havana, Cuba

[8] Centro de Investigaciones Energéticas Medioambientales y Tecnológicas (CIEMAT), Madrid, Spain

[9] Centro de Investigación y de Estudios Avanzados (CINVESTAV), Mexico City and Mérida, Mexico

[10] Centro Fermi – Centro Studi e Ricerche e Museo Storico della Fisica “Enrico Fermi”, Rome, Italy

[11] Chicago State University, Chicago, United States

[12] Commissariat à l’Energie Atomique, IRFU, Saclay, France

[13] Departamento de Física de Partículas and IGFAE, Universidad de Santiago de Compostela, Santiago de Compostela, Spain
[14] Department of Physics Aligarh Muslim University, Aligarh, India
[15] Department of Physics and Technology, University of Bergen, Bergen, Norway
[16] Department of Physics, Ohio State University, Columbus, Ohio, United States
[17] Department of Physics, Sejong University, Seoul, South Korea
[18] Department of Physics, University of Oslo, Oslo, Norway
[19] Dipartimento di Fisica dell'Università and Sezione INFN, Bologna, Italy
[20] Dipartimento di Fisica dell'Università and Sezione INFN, Padova, Italy
[21] Dipartimento di Fisica dell'Università and Sezione INFN, Trieste, Italy
[22] Dipartimento di Fisica dell'Università and Sezione INFN, Cagliari, Italy
[23] Dipartimento di Fisica dell'Università and Sezione INFN, Turin, Italy
[24] Dipartimento di Fisica dell'Università 'La Sapienza' and Sezione INFN, Rome, Italy
[25] Dipartimento di Fisica e Astronomia dell'Università and Sezione INFN, Catania, Italy
[26] Dipartimento di Fisica 'E.R. Caianiello' dell'Università and Gruppo Collegato INFN, Salerno, Italy
[27] Dipartimento di Scienze e Innovazione Tecnologica dell'Università del Piemonte Orientale and Gruppo Collegato INFN, Alessandria, Italy
[28] Dipartimento Interateneo di Fisica 'M. Merlin' and Sezione INFN, Bari, Italy
[29] Division of Experimental High Energy Physics, University of Lund, Lund, Sweden
[30] European Organization for Nuclear Research (CERN), Geneva, Switzerland
[31] Fachhochschule Köln, Köln, Germany
[32] Faculty of Engineering, Bergen University College, Bergen, Norway
[33] Faculty of Mathematics, Physics and Informatics, Comenius University, Bratislava, Slovakia
[34] Faculty of Nuclear Sciences and Physical Engineering, Czech Technical University in Prague, Prague, Czech Republic
[35] Faculty of Science, P.J. Šafárik University, Košice, Slovakia
[36] Frankfurt Institute for Advanced Studies, Johann Wolfgang Goethe-Universität Frankfurt, Frankfurt, Germany
[37] Gangneung-Wonju National University, Gangneung, South Korea
[38] Helsinki Institute of Physics (HIP) and University of Jyväskylä, Jyväskylä, Finland
[39] Hiroshima University, Hiroshima, Japan
[40] Indian Institute of Technology Bombay (IIT), Mumbai, India
[41] Indian Institute of Technology Indore (IIT), Indore, India
[42] Institut de Physique Nucléaire d'Orsay (IPNO), Université Paris-Sud, CNRS-IN2P3, Orsay, France
[43] Institute for High Energy Physics, Protvino, Russia
[44] Institute for Nuclear Research, Academy of Sciences, Moscow, Russia
[45] Nikhef, National Institute for Subatomic Physics and Institute for Subatomic Physics of Utrecht University, Utrecht, Netherlands
[46] Institute for Theoretical and Experimental Physics, Moscow, Russia
[47] Institute of Experimental Physics, Slovak Academy of Sciences, Košice, Slovakia
[48] Institute of Physics, Bhubaneswar, India
[49] Institute of Physics, Academy of Sciences of the Czech Republic, Prague, Czech Republic
[50] Institute of Space Sciences (ISS), Bucharest, Romania
[51] Institut für Informatik, Johann Wolfgang Goethe-Universität Frankfurt, Frankfurt, Germany
[52] Institut für Kernphysik, Johann Wolfgang Goethe-Universität Frankfurt, Frankfurt, Germany
[53] Institut für Kernphysik, Technische Universität Darmstadt, Darmstadt, Germany
[54] Institut für Kernphysik, Westfälische Wilhelms-Universität Münster, Münster, Germany
[55] Instituto de Ciencias Nucleares, Universidad Nacional Autónoma de México, Mexico City, Mexico
[56] Instituto de Física, Universidad Nacional Autónoma de México, Mexico City, Mexico
[57] Institut of Theoretical Physics, University of Wroclaw
[58] Institut Pluridisciplinaire Hubert Curien (IPHC), Université de Strasbourg, CNRS-IN2P3, Strasbourg, France
[59] Joint Institute for Nuclear Research (JINR), Dubna, Russia
[60] KFKI Research Institute for Particle and Nuclear Physics, Hungarian Academy of Sciences, Budapest, Hungary
[61] Kirchhoff-Institut für Physik, Ruprecht-Karls-Universität Heidelberg, Heidelberg, Germany

[62] Korea Institute of Science and Technology Information, Daejeon, South Korea
[63] Laboratoire de Physique Corpusculaire (LPC), Clermont Université, Université Blaise Pascal, CNRS–IN2P3, Clermont-Ferrand, France
[64] Laboratoire de Physique Subatomique et de Cosmologie (LPSC), Université Joseph Fourier, CNRS-IN2P3, Institut Polytechnique de Grenoble, Grenoble, France
[65] Laboratori Nazionali di Frascati, INFN, Frascati, Italy
[66] Laboratori Nazionali di Legnaro, INFN, Legnaro, Italy
[67] Lawrence Berkeley National Laboratory, Berkeley, California, United States
[68] Lawrence Livermore National Laboratory, Livermore, California, United States
[69] Moscow Engineering Physics Institute, Moscow, Russia
[70] National Institute for Physics and Nuclear Engineering, Bucharest, Romania
[71] Niels Bohr Institute, University of Copenhagen, Copenhagen, Denmark
[72] Nikhef, National Institute for Subatomic Physics, Amsterdam, Netherlands
[73] Nuclear Physics Institute, Academy of Sciences of the Czech Republic, Řež u Prahy, Czech Republic
[74] Oak Ridge National Laboratory, Oak Ridge, Tennessee, United States
[75] Petersburg Nuclear Physics Institute, Gatchina, Russia
[76] Physics Department, Creighton University, Omaha, Nebraska, United States
[77] Physics Department, Panjab University, Chandigarh, India
[78] Physics Department, University of Athens, Athens, Greece
[79] Physics Department, University of Cape Town, iThemba LABS, Cape Town, South Africa
[80] Physics Department, University of Jammu, Jammu, India
[81] Physics Department, University of Rajasthan, Jaipur, India
[82] Physikalisches Institut, Ruprecht-Karls-Universität Heidelberg, Heidelberg, Germany
[83] Purdue University, West Lafayette, Indiana, United States
[84] Pusan National University, Pusan, South Korea
[85] Research Division and ExtreMe Matter Institute EMMI, GSI Helmholtzzentrum für Schwerionenforschung, Darmstadt, Germany
[86] Rudjer Bošković Institute, Zagreb, Croatia
[87] Russian Federal Nuclear Center (VNIIEF), Sarov, Russia
[88] Russian Research Centre Kurchatov Institute, Moscow, Russia
[89] Saha Institute of Nuclear Physics, Kolkata, India
[90] School of Physics and Astronomy, University of Birmingham, Birmingham, United Kingdom
[91] Sección Física, Departamento de Ciencias, Pontificia Universidad Católica del Perú, Lima, Peru
[92] Sezione INFN, Trieste, Italy
[93] Sezione INFN, Padova, Italy
[94] Sezione INFN, Turin, Italy
[95] Sezione INFN, Rome, Italy
[96] Sezione INFN, Cagliari, Italy
[97] Sezione INFN, Bologna, Italy
[98] Sezione INFN, Bari, Italy
[99] Sezione INFN, Catania, Italy
[100] Soltan Institute for Nuclear Studies, Warsaw, Poland
[101] Nuclear Physics Group, STFC Daresbury Laboratory, Daresbury, United Kingdom
[102] SUBATECH, Ecole des Mines de Nantes, Université de Nantes, CNRS-IN2P3, Nantes, France
[103] Technical University of Split FESB, Split, Croatia
[104] The Henryk Niewodniczanski Institute of Nuclear Physics, Polish Academy of Sciences, Cracow, Poland
[105] The University of Texas at Austin, Physics Department, Austin, TX, United States
[106] Universidad Autónoma de Sinaloa, Culiacán, Mexico
[107] Universidade de São Paulo (USP), São Paulo, Brazil
[108] Universidade Estadual de Campinas (UNICAMP), Campinas, Brazil
[109] Université de Lyon, Université Lyon 1, CNRS/IN2P3, IPN-Lyon, Villeurbanne, France
[110] University of Houston, Houston, Texas, United States
[111] University of Technology and Austrian Academy of Sciences, Vienna, Austria
[112] University of Tennessee, Knoxville, Tennessee, United States
[113] University of Tokyo, Tokyo, Japan
[114] University of Tsukuba, Tsukuba, Japan

[115] Eberhard Karls Universität Tübingen, Tübingen, Germany
[116] Variable Energy Cyclotron Centre, Kolkata, India
[117] V. Fock Institute for Physics, St. Petersburg State University, St. Petersburg, Russia
[118] Warsaw University of Technology, Warsaw, Poland
[119] Wayne State University, Detroit, Michigan, United States
[120] Yale University, New Haven, Connecticut, United States
[121] Yerevan Physics Institute, Yerevan, Armenia
[122] Yildiz Technical University, Istanbul, Turkey
[123] Yonsei University, Seoul, South Korea
[124] Zentrum für Technologietransfer und Telekommunikation (ZTT), Fachhochschule Worms, Worms, Germany